ROTOR BLADE TREATMENTS TO MINIMIZE ELECTROSTATICALLY GENERATED NOISE ON THE HLH HELICOPTER

R. DeRosa, et al

Boeing Vertol Company

Prepared for:

Department of Defense

1 May 1974

AD220220

BOEING

AD 780 720
REV LTR

THE BOEING COMPANY

VERTOL DIVISION - PHILADELPHIA, PENNSYLVANIA

CODE IDENT. NO. 77272

NUMBER D301-10279-1

TITLE ROTOR BLADE TREATMENTS TO MINIMIZE ELECTROSTATICALLY GENERATED NOISE ON THE HLH HELICOPTER

ORIGINAL RELEASE DATE _____. FOR THE RELEASE DATE OF SUBSEQUENT REVISIONS, SEE THE REVISION SHEET. FOR LIMITATIONS IMPOSED ON THE DISTRIBUTION AND USE OF INFORMATION CONTAINED IN THIS DOCUMENT, SEE THE LIMITATIONS SHEET.

MODEL HLH CONTRACT DAAJ01-73-0017; Delivery Order 11

ISSUE NO. _____ ISSUED TO: _____

PREPARED BY R. DeRosa/J. Solak DATE _____

APPROVED BY T. Scarpati DATE _____

APPROVED BY R. Titus/G. Pries DATE _____

APPROVED BY G. Allen DATE 5/6/74

69

ACTIVE SHEET RECORD

SHEET NUMBER	REV LTR	ADDED SHEETS				SHEET NUMBER	REV LTR	ADDED SHEETS			
		SHEET NUMBER	REV LTR	SHEET NUMBER	REV LTR			SHEET NUMBER	REV LTR	SHEET NUMBER	REV LTR
1						36					
2						37					
3						38					
4						39					
5						40					
6						41					
7						42					
						43					
Appendix A						44					
1						45					
2						46					
3						47					
4						48					
5						49					
6						50					
7						51					
8						52					
9						53					
10						54					
11						55					
12						56					
13						57					
14						58					
15						59					
16						60					
17											
18											
19											
20											
21											
22											
23											
24											
25											
26											
27											
28											
29											
30											
31											
32											
33											
34											
35											

FORM 44139 07/83

LIMITATIONS

NONE

This document is controlled by HLH Blade Design

All revisions to this document shall be approved by the above noted organization prior to release.

TECHNICAL REPORT

This document was prepared by the Stanford Research Institute for the Boeing Vertol Company and is submitted to satisfy Contract Number DAAJ01-73-A-0017.

SRI Laboratory testing has shown the effect of dust and ice particles in generating static electricity on the blade surface. The electrical accumulations result in radio frequency noise interference.

Since the rotor blade paint coat is fabricated of materials which are electrically insulating, the first consideration is to render the blade surface electrically conductive. Several types of conductive paints were tested and are now available for this purpose. Test panels were fabricated, similar to blade structure, for evaluation of 13 different paint coating configurations. A noise reduction of 20 db from the noise level of the insulating paint system would cause interference to the LORAN-D guidance system, whereas a reduction of 40 db would provide noise-free operation of LORAN-D, with full range capability. Two of the paint systems which reduced the noise level by over 40 db from reference have been chosen for use on the HLH blade.

On the inboard blade shank, magna 3-B-6 is used with no overcoating required. This coating also provides erosion resistance to the fiberglass shank. On the blade fairing area, aft of the nose cap, BMS 10-21 conductive coating is used. The titanium nose cap, being conductive, does not require a conductive paint coating. The nose cap and fairing areas are then overlayed with epoxy primer and the acrylic nitrocelulose laquer paint system currently used on production rotor blades.

This combination of paints provides the erosion and moisture protection required on composite structures yet makes the blade electrically conductive, while providing in the field touch up capability.

A surface resistivity measurement technique has been devised which will allow a good in-service test method to assess the paint coat's ability to drain the surface charges noiselessly. Tests have shown a correlation of surface conductivity to noise reduction capability.

To prevent the helicopter potential, generated thru precipitation static, from reaching the corona discharge level, static dischargers, similar to those in use on production aircraft, are required. The discharger corona threshold (time at which discharge occurs) must obviously be lower than that of any rotor blade sharp edges. An area which requires attention is the tip of the rotor blade where the pressure reduction can cause the

TECHNICAL REPORT

Continued

outboard edge of the nose cap to reach it's corona threshold prior to the dischargers. The recommended configuration is to install two dischargers, on the trailing edge at the tip, and add a rounded tip cover with discharger installed. The design proposed for the HLH prototype will use two dischargers mounted on the trailing edge at the outboard end of the blade. These dischargers will be removable for shipment or replacement, with no special tools required. To reduce weight and cost, the present flat tip cover will be retained with provision for addition of a tip discharger if required.

Final Report

March 1974

SUPPORTING LABORATORY STUDIES FOR THE DEVELOPMENT OF ROTOR-BLADE TREATMENTS TO MINIMIZE ELECTROSTATICALLY GENERATED NOISE ON THE HLH HELICOPTER

By: J. E. KANEVSKY D. G. DOUGLAS

Prepared for:

THE BOEING COMPANY
VERTOL DIVISION, BOEING CENTER
P.O. BOX 16858
PHILADELPHIA, PENNSYLVANIA 19142

Approved by:

T. MORITA, Director
Electromagnetic Sciences Laboratory

RAY L. LEADABRAND, Executive Director
Electronic and Radio Sciences Division

Copy No. [illegible]

ABSTRACT

A laboratory investigation was undertaken to evaluate the severity of precipitation-static noise to be expected on the Heavy Lift Helicopter (HLH) low-frequency systems, and to define the requirements of techniques for noise elimination on the HLH.

This investigation, using a 1/25th scale model of the HLH and actual proposed rotor-blade panel samples revealed the need for EFI protection on the HLH. Recommendations were made to install P-static dischargers on the HLH rotor blades, and the optimum number and location of these dischargers was discussed.

Noise reduction afforded by various rotor-blade-coating systems was also investigated and reported. A recommendation was made for a particular coating system, based on noise-reduction and surface-resistivity measurements.

CONTENTS

ABSTRACT iii

LIST OF ILLUSTRATIONS vii

LIST OF TABLES ix

I INTRODUCTION 1

II NOISE-COUPLING ANALYSIS 5

III ELECTROSTATIC MODELING 19

IV BLADE-COATING TESTS 31

V CONCLUSIONS AND RECOMMENDATIONS 47

Appendix—REQUIREMENTS FOR ELECTRICALLY CONDUCTIVE BLADE COATINGS 51

REFERENCES 59

ILLUSTRATIONS

1	Possible LF and HF Antenna Locations Considered in Tests.	6
2	Test Setup for Coupling Measurements.	7
3	Antenna Coupling.	9
4	Noise at Antenna Location 1	12
5	Noise at Antenna Location 2	13
6	Noise at Antenna Location 3	14
7	Noise at Antenna Location 4	15
8	Corona Noise Levels at 707 Tailcap Antenna.	17
9	Arrangement for Determining Relationship Between Helicopter Potential and Reference-Point Field.	20
10	Setup to Determine Reference-Point Field Corresponding to Corona Threshold	21
11	Threshold Potentials of ELE Blade Structure	22
12	Reference-Point Fields for ELE Potential of 100 kV.	25
13	Space-Charge-Limited Discharge from End of Cylinder	26
14	Recommended Discharger Installations on ELE Blades.	29
15	Test Setup Used in Blade-Coating Tests.	31
16	Test-Sample Details	33
17	Tracks of Streamer Discharges Generated on Non-conductively Coated Test Panel.	35
18	Coaxial Conductivity Probe Used to Determine the Electrical Conductivity of Various ELE Blade Panels	40
19	Photograph of Typical Blade Sample with BMS 10-21 Base Material (10X)	41
20	Photograph of Surface of Sample 2 (30X)	42

21 High-Voltage Conductivity of ELB Blade Panels with Magna S-B-6 Base Material. 44

22 Photograph of Typical ELB Blade Panel Surface with Magna S-B-6 Conductive Base Coat 45

A-1 Current Flow in Surface Conducting Film 54

TABLES

1	Description of Blade-Material Test-Panel Coatings	36
2	Results of Blade-Sample Charging Studies.	37
3	Comparison of Noise Reduction and Surface Resistivity of Panels with BMS 10-21 Base Coat.	42

I INTRODUCTION

When communication and navigation equipment was first installed on aircraft, the aircraft operators found that radio noise was observed in these systems whenever the aircraft was operated in clouds of dust or precipitation.[1-4]* These early investigators found that the noise stemmed from frictional electrification of the aircraft as a whole or of individual parts as particles in the cloud struck the aircraft and deposited increments of charge. The problem subsequently was studied in considerable detail to identify the noise mechanisms responsible and to devise schemes for reducing the noise to tolerable levels.[5-11] Many techniques have been developed and applied to conventional aircraft.

Static electrification occurs on helicopters also when they are operated in clouds of dust or snow. The most serious problem recognized in connection with helicopter operation was the electrostatic discharge to ground during cargo operations,[12] where it was found that personnel were sometimes knocked off their feet by shock and suffered miscellaneous injuries such as split tips and edges of fingers and nails. Various active schemes were tried to eliminate the static charge on helicopters.[13-16] In a joint SRI-Boeing Vertol investigation, it was concluded that the charge on the dust cloud stirred up by the hovering helicopter completely dominated the electrostatic environment, and that it would not be possible to sense helicopter-to-ground potential without touching the ground. Accordingly, a passive aircraft grounding scheme was devised and demonstrated.[17]

---

*References are listed at the end of the report.

In addition to cargo-handling problems caused by electrification, helicopters are also subject to the noise problems encountered in conventional aircraft. In this regard, the helicopter is no different. Electrification will occur, and radio noise will result. In the case of the HLH, the problem of radio noise became of particular significance with the development of modern low-frequency navigational aids such as LORAN D, which operates at roughly 100 kHz. These systems provide capabilities that cannot be achieved in any other way. Since they operate at LF, however, they are particularly vulnerable to precipitation-static interference.

It was recognized that most precipitation-static fixes are simple and inexpensive to implement if they are considered as part of the vehicle design. As retrofits, these same fixes often become so expensive as to preclude their consideration. Accordingly, this program was instituted to investigate the severity of precipitation-static noise to be expected on the HLH and to define the requirements for techniques for noise elimination on the HLH helicopter.

In conversations with Boeing Vertol personnel, various approaches were discussed for eliminating radio-frequency noise stemming from frictional electrification of the HLH helicopter. During these discussions it was concluded that the most promising approach to noise elimination was through proper design and treatment of the helicopter blades.

Electrification of the vehicle as a whole leads to high electric fields and corona discharges at the rotor extremities.[5,8,10] Noise from this source can be eliminated by installing, at the rotor tips, passive dischargers capable of providing sufficient noise reduction to bring the resulting corona-noise levels down to acceptable values.[9,11] In planning such a discharger installation, it is necessary to specify the noise reduction required of the dischargers. It is also necessary to

define the number of dischargers required and to specify their locations on the rotor blades.

Charging of the plastic blade surfaces as the result of impact by snow or dust causes charge to accumulate on the surface of the blade until streamer discharges occur over the blade surface to some metallic structure to relieve some of the charge. These discharges also generate RF noise that can disable radio communication and navigation systems.[6,7] Streamer noise is best eliminated by applying a coat of conductive paint to the surface of the blade to remove the charge as rapidly as it arrives on the blade.[7] In this way, the high electric fields that lead to streamer discharges are eliminated.

In general, conductive paint is produced by adding conductive powder (metal or graphite) to a paint vehicle until the desired conductivity is achieved. This usually requires so much powder that the mechanical properties of the paint are degraded. For this reason, it is planned that, on the HLH, the conductive paint will be overcoated with a thin layer of nonconductive paint having the desired mechanical and abrasion-resistant properties. The argument is that this thin outer layer of paint will puncture at low voltages and permit the charge accumulating on the outer surface to flow to the conductive layer without generating large streamer discharges on the outside surface. It was necessary to test the workability of various materials that were selected for this function.

It was concluded that the needs of the HLH could be met by accomplishing the following three tasks on the present program:

(1) Conduct the necessary model coupling measurements and analyses to determine the discharger-noise reduction required to afford the same degree of noise protection for the HLH as is currently available on airliners such as the 707 using LORAN C/D.

(2) Conduct the necessary electrostatic model measurements and analyses to establish the number and placement of passive dischargers on the HLH rotor blades.

(3) Conduct triboelectric charging tests on as many as 10 samples of candidate conductive coating systems to determine their adequacy for use on the HLH rotor blades.

Since the noise problem has been studied at great length on conventional aircraft, extensive use will be made here of this earlier work. In particular, reference will be made to specific equations and techniques developed in previous publications. Generally, the required equation will be abstracted and used without rederivation or extensive justification. Attempting to justify every step here would result in an inappropriately long and complex report.

II NOISE-COUPLING ANALYSIS

As indicated in the Introduction, static electrification of the helicopter as a whole raises its potential until corona discharges occur from the regions of highest electric field at the rotor tips. These discharges generate radio noise that couples into receiving systems on the vehicle. Similarly, charging of the dielectric outer surfaces of the blades will result in streamer discharges across the surfaces that also couple noise into receiving systems. The severity of the resulting interference must be estimated in order to weigh the importance of developing fixes. Thus, it is necessary to determine the degree of coupling between noise sources on the blades and regions on the HLH where antennas might be located.

Positions where antennas might conceivably be located on the HLH and where coupling measurements were made are shown in Figure 1. Position 1 is on the lower part of the nose, where antennas could clearly be located without difficulty. The feasibility of antenna locations such as those in positions 2 and 3 on the top of the fuselage depends on the degree to which performance of the associated system will be degraded by rotor-blade modulation. It was felt that such installations were definitely possible, and that measurements of noise coupling to this general region should be made. Another clear area where antennas might be installed was the back of the aft pylon. Accordingly, measurements were made of coupling to position 4. Since the HLH design incorporates provisions for carrying large container cargoes along the flat part of the belly, it will not be possible to install antennas here. For this reason, no measurements of coupling to this part of the belly were made.

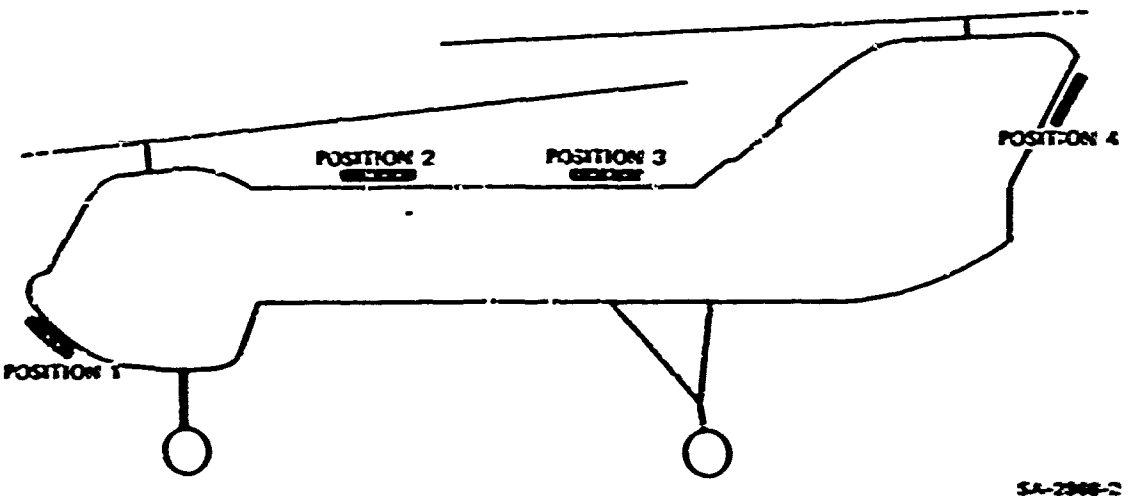

FIGURE 1 POSSIBLE LF AND HF ANTENNA LOCATIONS CONSIDERED IN TESTS

The measurement techniques used in the present program were patterned after those described in Ref. 8. The test setup is shown in Figure 2. Here a miniature RF oscillator is shown in position at the end of one of the rotor blades. DC power is fed to the oscillator via a high-resistance lead that is of sufficiently high value to appear transparent at the RF frequencies of interest. The power-supply ground return from the helicopter is made via a second high-resistance lead. Thus the setup simulates an electrically isolated helicopter with a small, isolated RF generator at the tip of one of its blades.

Noise picked up by the test antenna on the aircraft is fed to an attenuator followed by a battery-operated receiver tuned to the oscillator frequency. The attenuator is adjusted to produce a standard reading in the meter connected to the receiver output. The meter is also contained in the model and is read optically. To obtain absolute values of coupling, the RF source is placed against the inner conductor of the standard coaxial coupling structure, which is attached to the receiving system in place of the test antenna. The attenuator is adjusted to produce the standard reading on the receiver output meter. In this way the ratio of

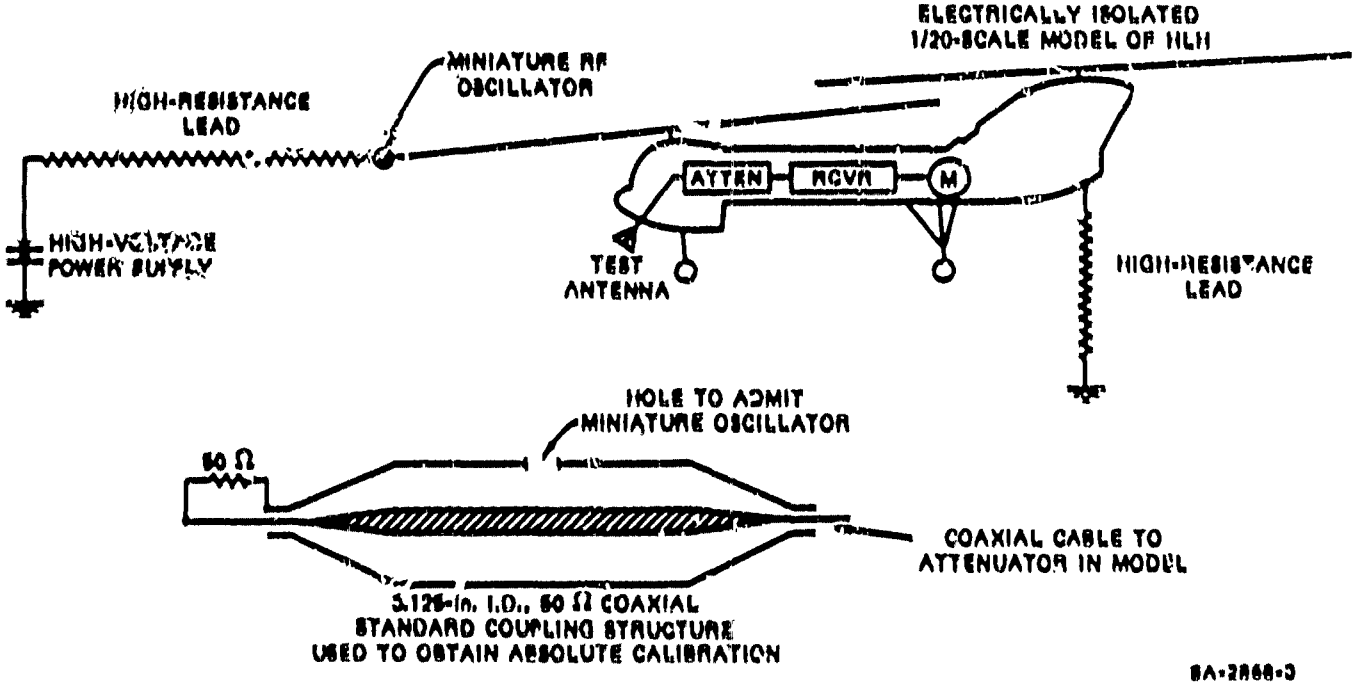

FIGURE 2 TEST SETUP FOR COUPLING MEASUREMENTS

the measured coupling to the standard coupling is given by the ratio of the attenuation settings required to produce the standard receiver output.

It is recognized, of course, that in performing the coupling measurements as described, the characteristics of the receiving antenna used on the model are automatically incorporated in receiver output and measured coupling. To make the measurements more generally useful therefore, the test antenna properties have been removed from the results using antenna data developed by Bolljahn.[18] Additional discussion of this procedure is given in Ref. 8. The results of the EME coupling measurements shown in Figure 3(a) through 3(d) are presented in terms of coupling to an antenna of unit induction area. Thus the coupling data can be thought of as expressing the coupling between a discharge source on a blade, and a location on the helicopter where one might wish to locate a receiving antenna. The coupling to an actual antenna considered for use can be determined simply by multiplying the normalized coupling factor of Figure 3 by the antenna induction area. In determining the induction area, a, of a particular antenna it is convenient to use the relationship

$$c_o a = h_e C \quad .$$

where

$$c_o = \frac{1}{36\pi \times 10^9} \text{ F/m}$$

a = Antenna induction area

$h_e C$ = Antenna sensitivity product.

Thus, for a typical sense antenna having a sensitivity product $h_e C = 4$ pFm, the induction area is $a = 4 \times 10^{-12}(36\pi \times 10^9) = 0.45 \text{ m}^2$.

It is evident from Figure 3 that the measurements were confined to frequencies below 2.5 MHz. This restriction was imposed because the

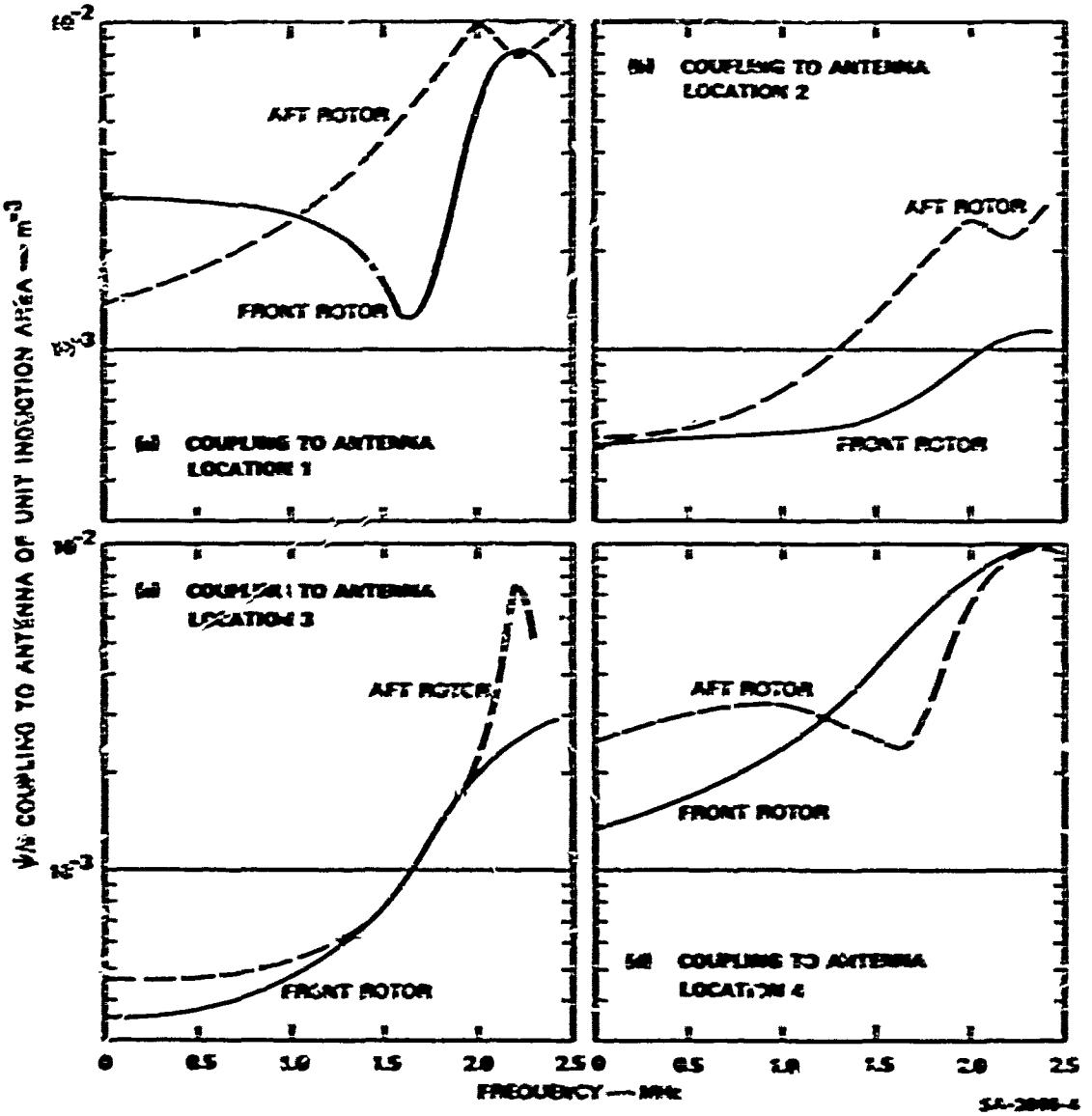

FIGURE 3 ANTENNA COUPLING

primary concern in this program was systems operating in the LF portion of the spectrum. To generate confidence in the data, however, the measurements were extended to the low part of the HF regime where aircraft resonances should begin to manifest themselves in the coupling magnitudes. For example, in Figure 34 of Ref 5, Tanner shows analytically that the first maximum in noise coupling from the long end of an asymmetrical dipole occurs when the length of the long half is 0.375λ. Considering the coupling between the position-1 antenna and a discharge on the end of the aft rotor, the first maximum should occur when the distance between the nose of the helicopter and the aft rotor-blade tip, a distance of roughly 133 ft (for θ = 180°), is 0.375λ. This corresponds to a frequency of 2.8 MHz. From Figure 3(a), we see that the measured coupling from the aft rotor to antenna position 1 is increasing with increasing frequency up to the highest frequency measured in the laboratory tests.

It should also be observed that only one coupling curve is presented for each rotor. Measurements were actually made for five blade positions, but it was found that the coupling data changed very little after the blade was 90° or more removed from the fuselage. (As will be seen in the next section, this is the blade location in which corona discharges will occur.) Accordingly, to simplify the presentation and the calculations, a single composite curve of coupling is presented for each rotor in Figure 3.

In general, the coupling data of Figure 3 have the same behavior as the 707 low-frequency coupling data of Ref. 8. The coupling is relatively flat at low frequencies, and exhibits various resonances and antiresonances at the higher frequencies. No effort has been made to account for the details of the variations measured. The EM structure is sufficiently complex that attempts in this direction are not likely to be fruitful.

The coupling data of Figure 3 were used together with the corona-noise spectral data of Ref. 3 to generate the curves of corona-noise equivalent field shown for the various antenna positions in Figure 4 through 7. (Streamer noise also shown in these figures will be discussed later in this section.) In carrying out these calculations, it was assumed that the helicopter charging current was 600 μA, and that it split equally between the two rotors. The noises generated from the two rotors were added on an rms basis to determine the total noise current induced in the antenna. Following the procedures of Ref. 8, the noise current was then expressed in terms of the equivalent noise field required at the antenna location to produce the same short-circuit antenna current.

Essentially, the data of Figures 4 through 7 show the noise fields that would exist at the antenna locations on the HLH if it were operated without dischargers on the rotor blades in a region of severe charging.

Using the coupling data of Figure 3 again, but this time in conjunction with streamer-noise data of Ref. 7, calculations were made to determine the level of noise that would exist at the antenna locations if the rotor blades were untreated and 600 μA of charging to the blade surfaces returned to the metallic structure of the blades via streamer discharges over the surface. The results of these calculations are presented for the various antenna-positions in Figures 4 through 7.

Also shown in Figures 4 through 7 are levels of atmospheric noise field obtained from Ref. 19 and adjusted for a 1-kHz bandwidth. The corona and streamer noise fields are seen to be 40 to 60 dB greater than the atmospheric noise throughout the entire frequency range considered in the case of antenna positions 1 and 4. The noise is somewhat less severe in the case of antenna positions 2 and 3. The implications of noise on the operation of LORAN-D systems are as follows: The LORAN-D system designer can achieve improved system performance until he has reduced

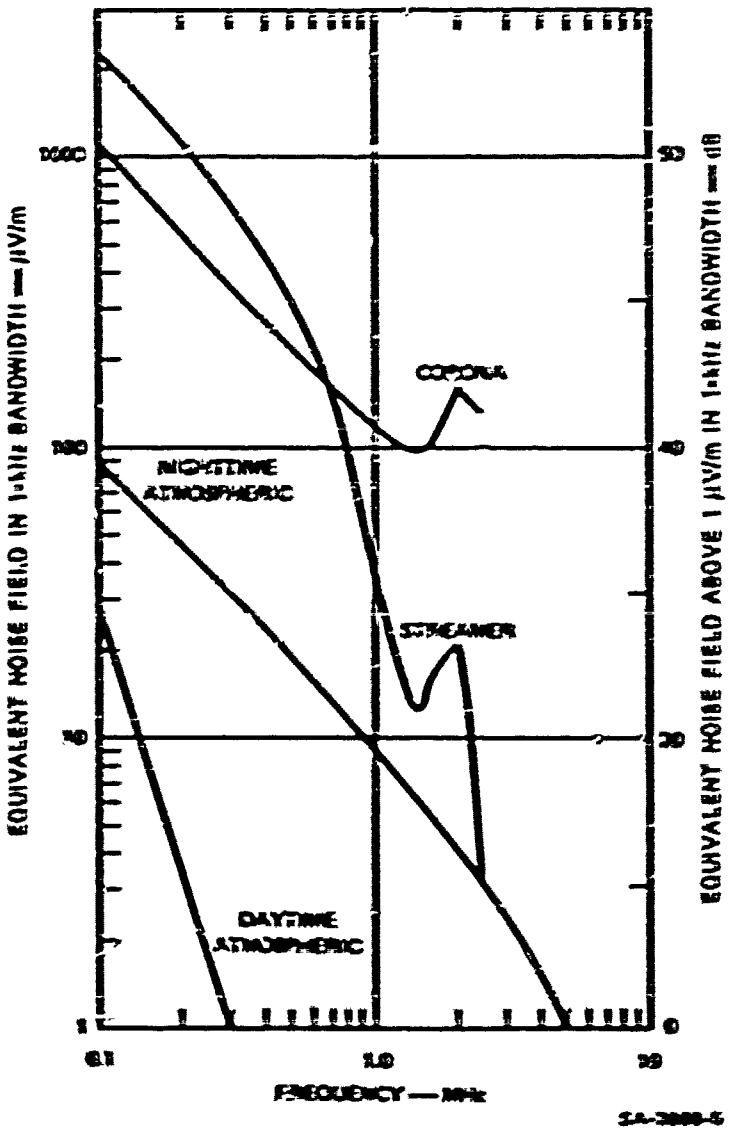

FIGURE 4 NOISE AT ANTENNA LOCATION 1

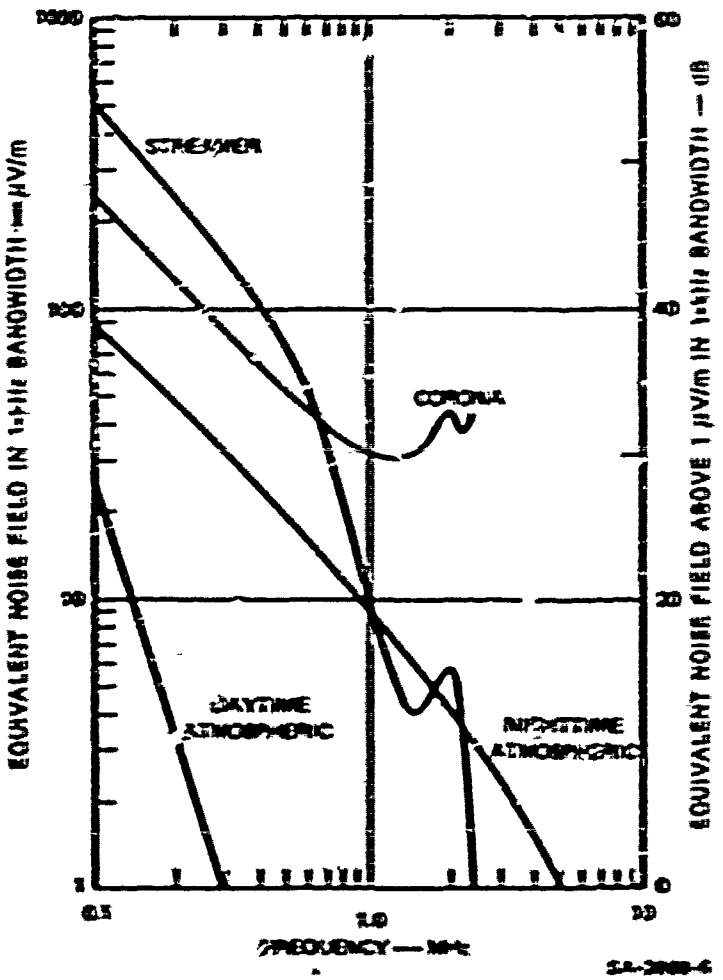

FIGURE 5 NOISE AT ANTENNA LOCATION 2

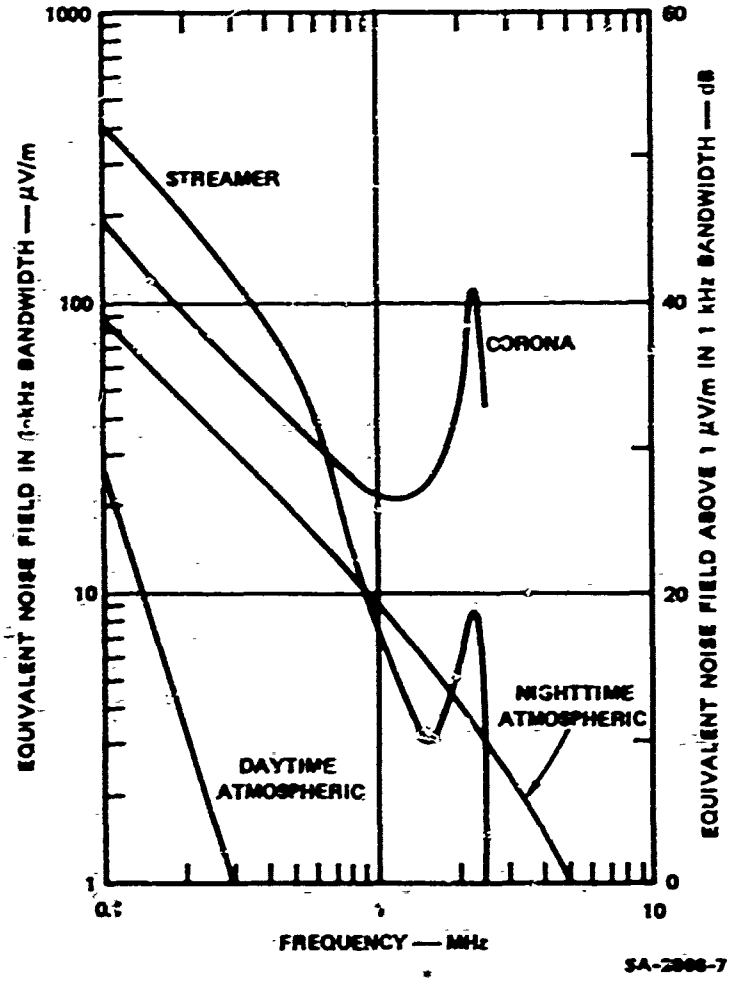

FIGURE 6 NOISE AT ANTENNA LOCATION 3

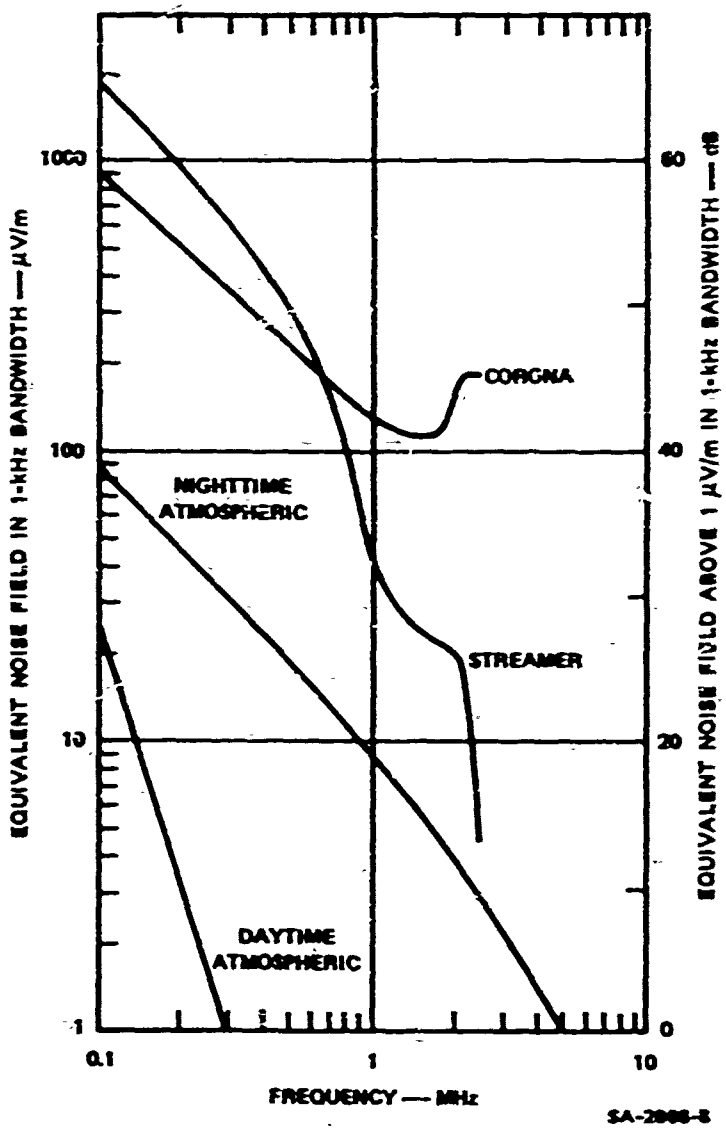

FIGURE 7 NOISE AT ANTENNA LOCATION 4

his system input noise figure to the atmospheric noise level. From this observation we can infer that such systems are now, or ultimately will be, operating at the atmospheric noise level limit. From Figures 4 through 7, we see that corona or streamer noise from the blades will severely degrade the performance of such a system. In particular, the analysis indicates that from 20 to 40 dB of noise reduction is required to reduce the electrostatically generated noise levels to the daytime atmospheric level.

Shown in Figure 8 for comparison are corona-noise fields at the 707 tailcap antenna location for two conditions. In the first, corona discharges are permitted to occur from the rudder, resulting in high coupling to the antenna and high equivalent noise fields. Eliminating the discharges from the rudder has the effect of reducing the noise levels to the values given by the lower curve. The data of Figure 8 were verified in the series of flight tests described in Refs. 8 and 9.

It should be noted at this time that in order to achieve satisfactory operation of communication and navigation equipment, aircraft such as the 707 are equipped with dischargers capable of providing 45 to 60 dB noise reduction, and the dischargers are numerous enough and in sufficiently effective locations to permit all of the charging current to leave the aircraft. To reduce electrostatically generated noise to similar levels on the HLH, it will be necessary to provide comparable degrees of noise reduction to both streamer and corona-interference sources.

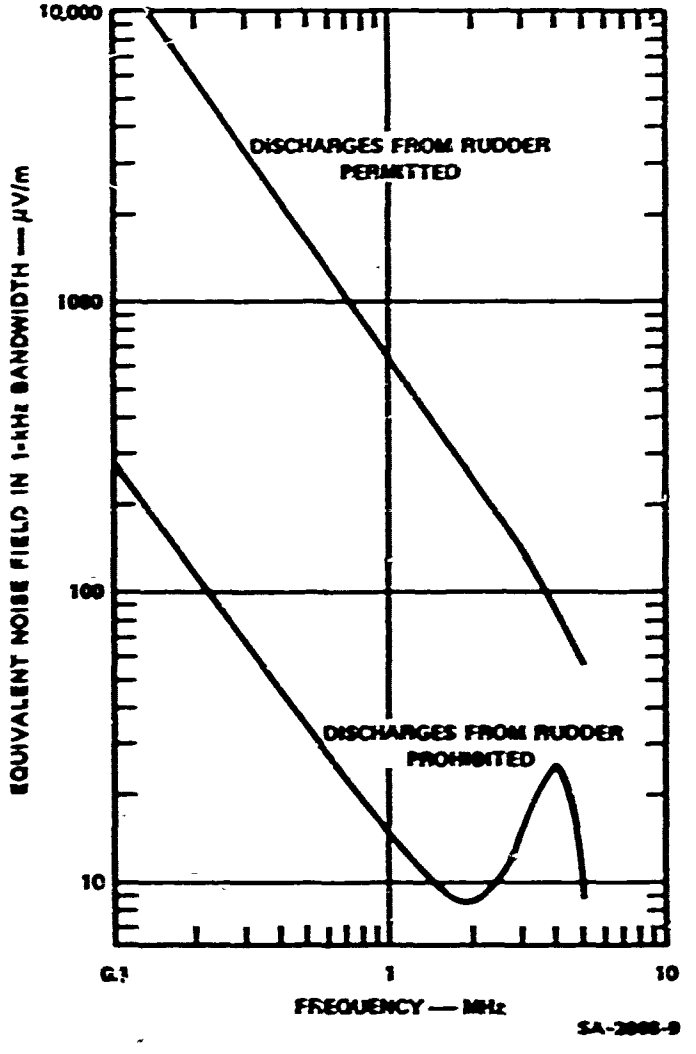

FIGURE 8 CORONA NOISE LEVELS AT 707 TAILCAP ANTENNA

III ELECTROSTATIC MODELING

Laboratory electrostatic measurements were made to determine corona thresholds of the HLH blades, and to estimate discharge currents from passive dischargers located on the blades. The measurements were carried out in two steps. First, the setup illustrated in Figure 9 was used to determine the relationship between the helicopter potential and a reference on a helicopter blade as a function of angle θ with respect to the fuselage. (The reference point chosen was 12 inches inboard of the tip and 12 inches forward of the trailing edge on the full-scale vehicle.)

In carrying out the measurements illustrated in Figure 9, the 1/48-scale model was sprayed with conducting silver-loaded paint to render it conducting. The model was suspended in the laboratory and connected to a high-voltage power supply. A small metal probe mounted on a thin, electrically insulating handle was touched to the blade at the reference point. The charge acquired by the probe was transferred to a Faraday "ice pail" attached to the input of an infinite-impedance electrometer.

The relationship between probe charge and surface field was determined by repeating the charge-transfer measurement in the known surface field between a pair of metal plates where the field is given by

$$E = V/d$$

where

V = Applied voltage

d = Spacing between plates.

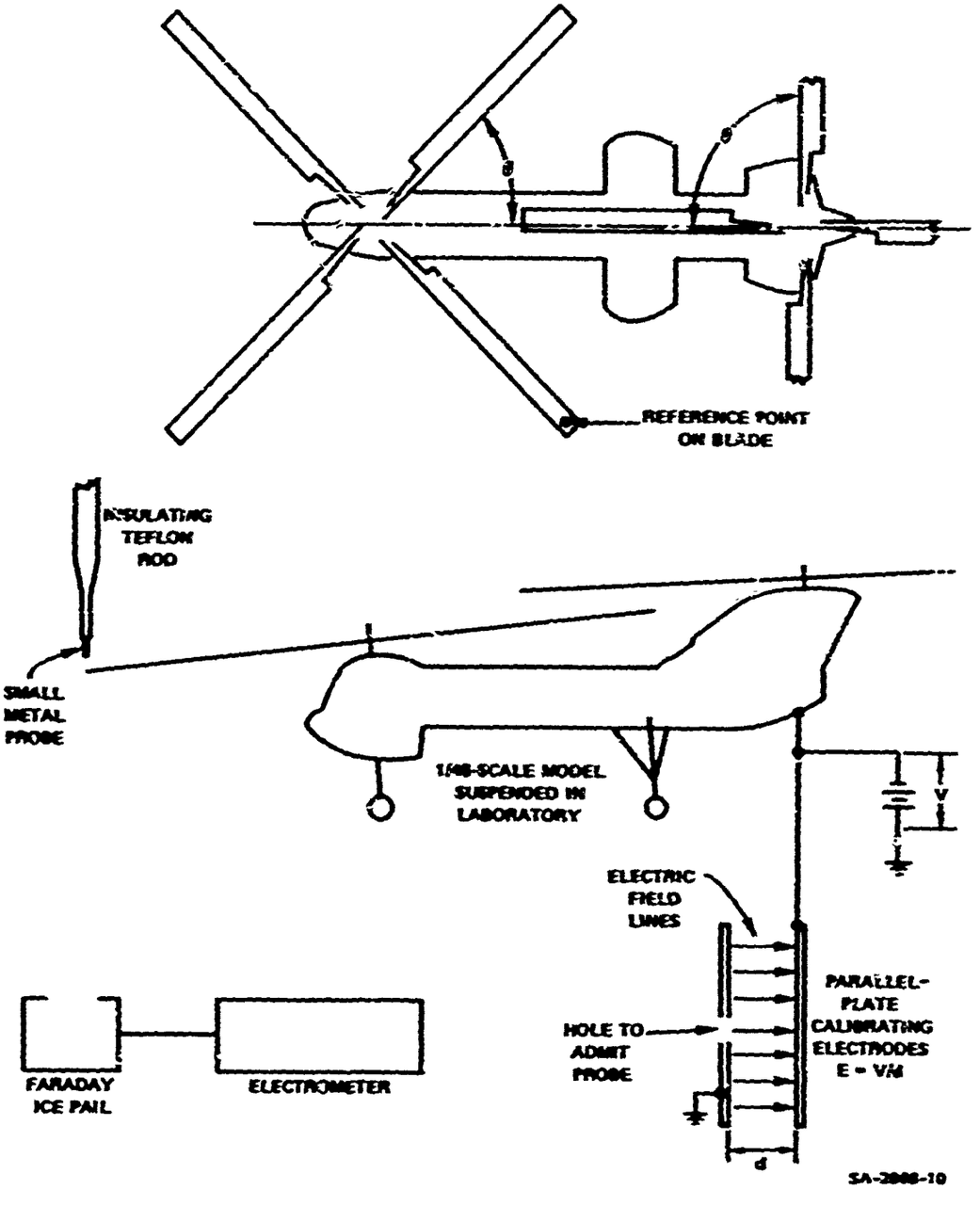

FIGURE 9 ARRANGEMENT FOR DETERMINING RELATIONSHIP BETWEEN HELICOPTER POTENTIAL AND REFERENCE-POINT FIELD

In the second step of the electrostatic studies, a full-scale section of HLH helicopter rotor blade was suspended in the laboratory as illustrated in Figure 10. The power-supply voltage was increased until corona onset occurred (a corona current of 20 μA was used to indicate onset). The reference-point field at threshold was then measured in the setup of Figure 10. Since the earlier experiments using the setup of Figure 9 developed a relationship between reference-point field and helicopter potential it is now possible to state the potential at which corona threshold will occur as a function of blade position.

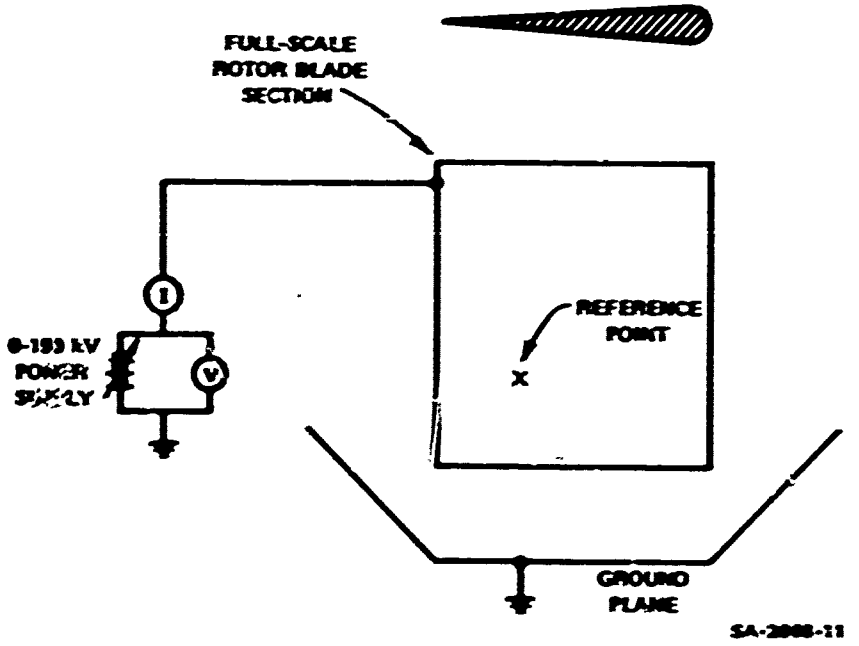

FIGURE 10 SETUP TO DETERMINE REFERENCE-POINT FIELD CORRESPONDING TO CORONA THRESHOLD

Figure 11 shows the result of the corona-threshold measurements made in the laboratory. It is evident that the threshold is sensitive to blade position. In particular, minimum threshold occurs when $\theta = 180°$, and the threshold increases markedly when the blade is shielded by the fuselage (for $\theta < 45°$). The shielding effect on the forward rotor blades

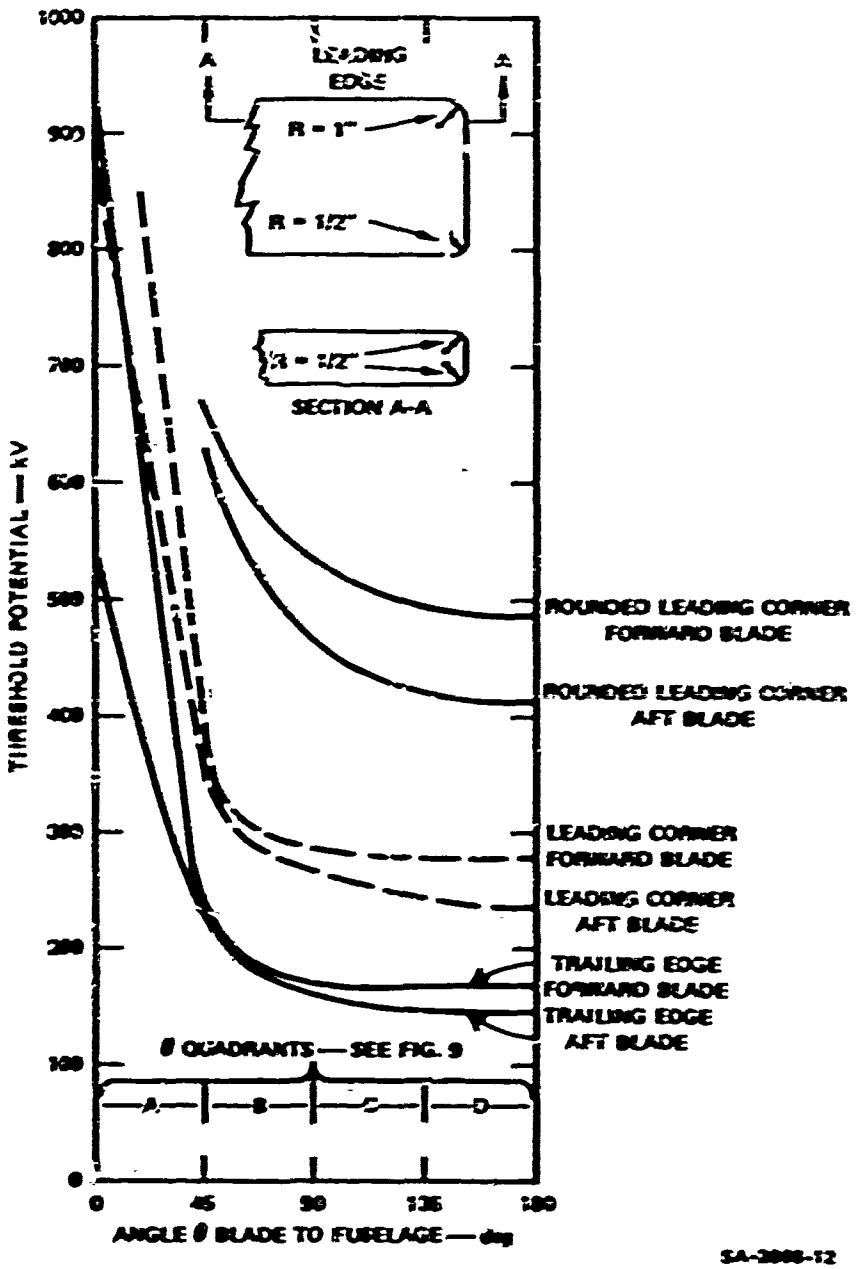

FIGURE 11 THRESHOLD POTENTIALS OF HLH BLADE STRUCTURE

is more pronounced than on the aft rotor because the forward rotor blades pass closer to the fuselage (see Figure 9).

The trailing edge of the aft blade has the lowest minimum corona threshold (roughly 150 kV). The minimum threshold of the forward rotor is somewhat higher, but still substantially below the threshold of the leading corner of either blade (250 to 275 kV). As is evident from Figure 11, some experimentation was done to determine the effect of installing a rounded cap on the tip of the blade. The cap has the effect of greatly increasing the corona threshold of the leading corner of the rotor (425 to 455 kV). The implications of these measurements will be dealt with later.

The fact that corona threshold increases so rapidly for $\theta < 45°$ means that most discharging will occur for $\theta > 45°$.

The implications of Figure 11 should be considered further. For $\theta = 180°$, with no dischargers installed, and with no airflow to generate localized pressure reductions, the model studies indicate that corona threshold of the blade-tip trailing-edge structure will occur when the vehicle potential reaches 150 kV. Assuming that the blades are equipped with trailing-type passive dischargers of the sort used on commercial transport aircraft, corona threshold of the dischargers will occur at roughly 1/10 the threshold of the trailing edge itself. Thus, long before trailing-edge threshold is approached, the dischargers function and generate columns of space charge that have the effect of shielding the blade trailing edge proper, thereby increasing its corona threshold by as much as a factor of 2 to a potential of, say, 250 to 300 kV (see Figure 43 of Ref. 8). Thus the model measurements indicate that, with trailing dischargers installed, corona threshold of the blade trailing edge and blade leading corner will occur at 250 to 300 kV, assuming that there are no vortices present to produce localized pressure reductions (which

reduce corona threshold in proportion to pressure reduction). This means that we cannot under any circumstance allow the helicopter voltage to approach 250 to 300 kV because if it does, noise-producing corona discharges will occur from the blade structure.

Let us now assume that we find a factor-of-2.5-to-3 margin of safety in vehicle voltage acceptable (this means that we feel confident that the combination of uncertainties in localized pressure reduction and errors in our laboratory studies is less than 2.5 to 3). Let us estimate the current that would be discharged by a minimal installation of two trailing dischargers per blade when the helicopter potential is 100 kV. (The dischargers are assumed to be 6 to 7 inches long in the manner of an ortho-decoupled discharger as described in Refs. 8, 9, and 11.) First, using the results of the reference-point-field measurements, we determine the reference-point field as a function of blade position for an aircraft potential of 100 kV. The results of such a determination are shown in Figure 12.

In Eq. (31) of Ref. 8, an expression is given for the space-charge-limited current discharged from the end of a rod capped with a zero-threshold ion source and placed in a windstream (see Figure 13). (The validity of this expression was verified in flight for the case of ortho-decoupled dischargers, which have a corona threshold roughly 1/10 that of the sharp trailing edge on which they are mounted.) The equation is:

$$i = W a E_a 2\pi\epsilon_o \qquad (1)$$

where

i = Discharge current

W = Windspeed, m/s

a = Radius of discharger cylinder

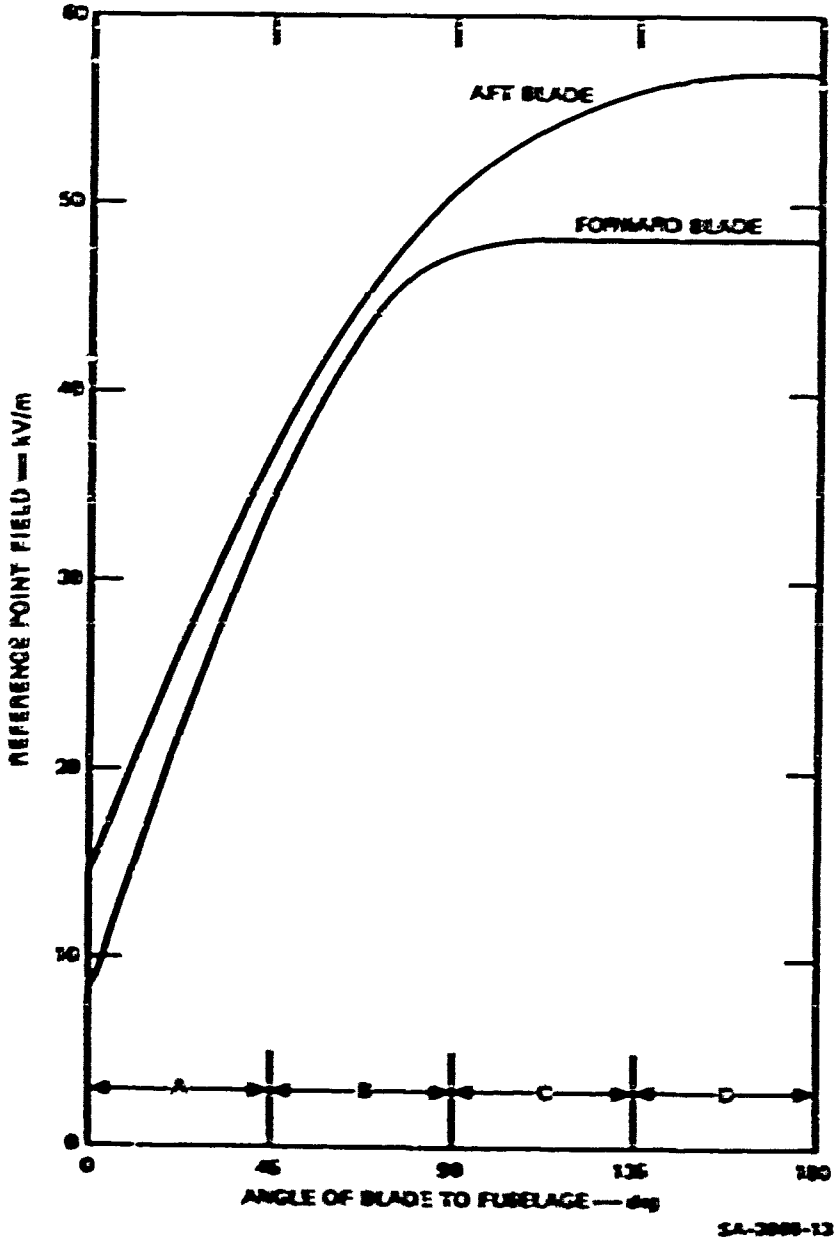

FIGURE 12 REFERENCE-POINT FIELDS FOR HIGH POTENTIAL OF 100 kV

E_a = Field intensity at surface of rod, V/m

$\epsilon_0 = 1/36\pi \times 10^{9}$ farad/m.

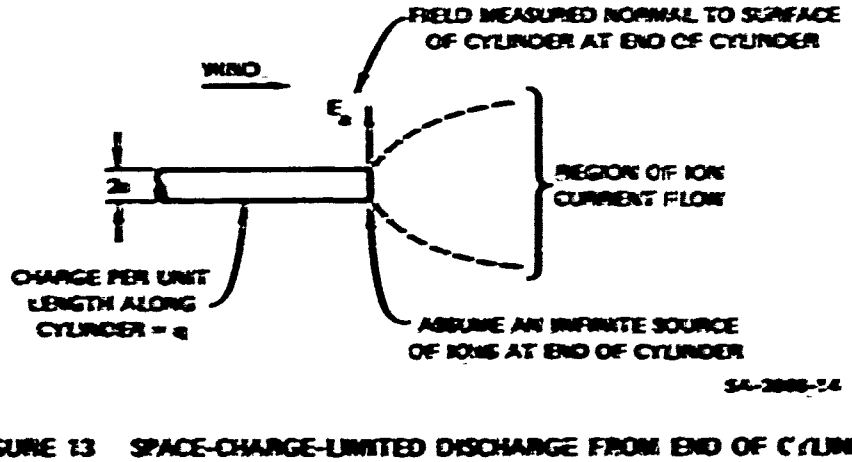

FIGURE 13 SPACE-CHARGE-LIMITED DISCHARGE FROM END OF CYLINDER

First we note that Eq. (1) is linear with E_a. Thus it is permissible to average E_a over the active portion of a blade rotation and to calculate i from the average E_a. We will start by finding an average reference-point field $\bar{E}_R$ and converting this to an average E_a. Let us average E_R over quadrants B, C, and D in Figure 12 using linear interpolation between end points of the quadrants. This averaging yields

$$\bar{E}_R = 49 \text{ kV/m} \quad .$$

Arguments along the lines of those on p. 91 of Ref. 8 indicate that for the HLH blade, $\bar{E}_a/\bar{E}_R = 25.9$. Thus, for 100 kV on the HLH,

$$\bar{E}_a = 1.27 \times 10^{6} \text{ V/m} \quad .$$

Let us assume that the tip of the rotor has a velocity of 250 m/s (this corresponds to a speed of $\lambda = 0.75$, which is conservatively below the

Mach = 1 limit for helicopter blades). Let us also choose 2a = 1/4 inch = 6.35×10^{-3} m. Substituting all these values into Eq. (1) yields

$$i = \frac{250(6.35 \times 10^{-3})(1.27 \times 10^{6})\ 2\pi}{2(36\pi \times 10^{9})}$$

$$= 56\ \mu A \quad .$$

Since both dischargers on the blade should discharge roughly the same current, and since only dischargers in quadrants B, C, and D are active, the total current discharged by this compliment at a helicopter potential of 100 kV is

$$I_{Total} = 12(56)$$

$$= 672\ \mu A \quad .$$

This is slightly in excess of the 600-μA peak charging current postulated for the HLH helicopter.

Let us now consider the design of discharger installations suitable for HLH. The above calculated value of total discharge current means that two trailing dischargers per blade can reasonably be expected to handle the maximum anticipated charging current to the HLH while holding the vehicle potentials below 100 kV. The results obtained above also indicate that in the absence of localized pressure reductions, none of the blade structure should reach corona threshold until the vehicle potential is in the range 250 to 300 kV. Flight-test experience on jet aircraft, however, indicates that substantial pressure reductions do occur at the ends of airfoils, permitting corona discharges at potentials substantially below those predicted on the basis of still air measurements.[8,9] For example, it was found that noise onset occurred when the

aircraft potential was 1.3 times the trailing-edge threshold (see p. 147 of Ref. 8). This result was obtained with rounded tips on the airfoils. Satisfactory operation of passive discharger systems on conventional aircraft was not achieved until airfoil-tip dischargers were developed to generate a column of space charge along the tip of the airfoil to provide shielding and a corresponding corona-threshold increase in the regions where localized pressure reductions can occur.[8,9] In light of this jet aircraft experience, it appears prudent to anticipate similar conditions on the HLH blades and to take steps in the initial blade design to circumvent them.

The preferred discharger installation is shown in Figure 14(a). Here, two trailing dischargers are provided to handle the bulk of the discharge current. A rounded tip cap is installed on the end of the blade to increase corona thresholds at the tip of the blade. In particular, rounding increases the threshold of the leading corner by a factor of 2, and eliminates the sharp edges along the top and bottom of the blade tip, thereby increasing the overall corona thresholds in the entire tip region of the blade. A tip-type discharger installed on the rounded cap results in the generation of a cloud of space charge along the rotor blade tip to raise corona thresholds even further. Thus the installation of Figure 14(a) is designed to take into account all of the corona sources that experience on jet transports indicates are likely to occur, and incorporates provisions for reducing the likelihood of their occurrence.

If the tip modifications required to accomplish the installation of Figure 14(a) impose unacceptable weight, drag, or cost penalties, it is possible to simplify the installation somewhat to the one illustrated in Figure 14(b), with some attendant loss of performance. Here the normal squared-off blade tip is retained, and three dischargers are installed as illustrated. Removing the rounded tip cap reduces the thresholds of the front blade corner to roughly 250 kV in still air. Also eliminating

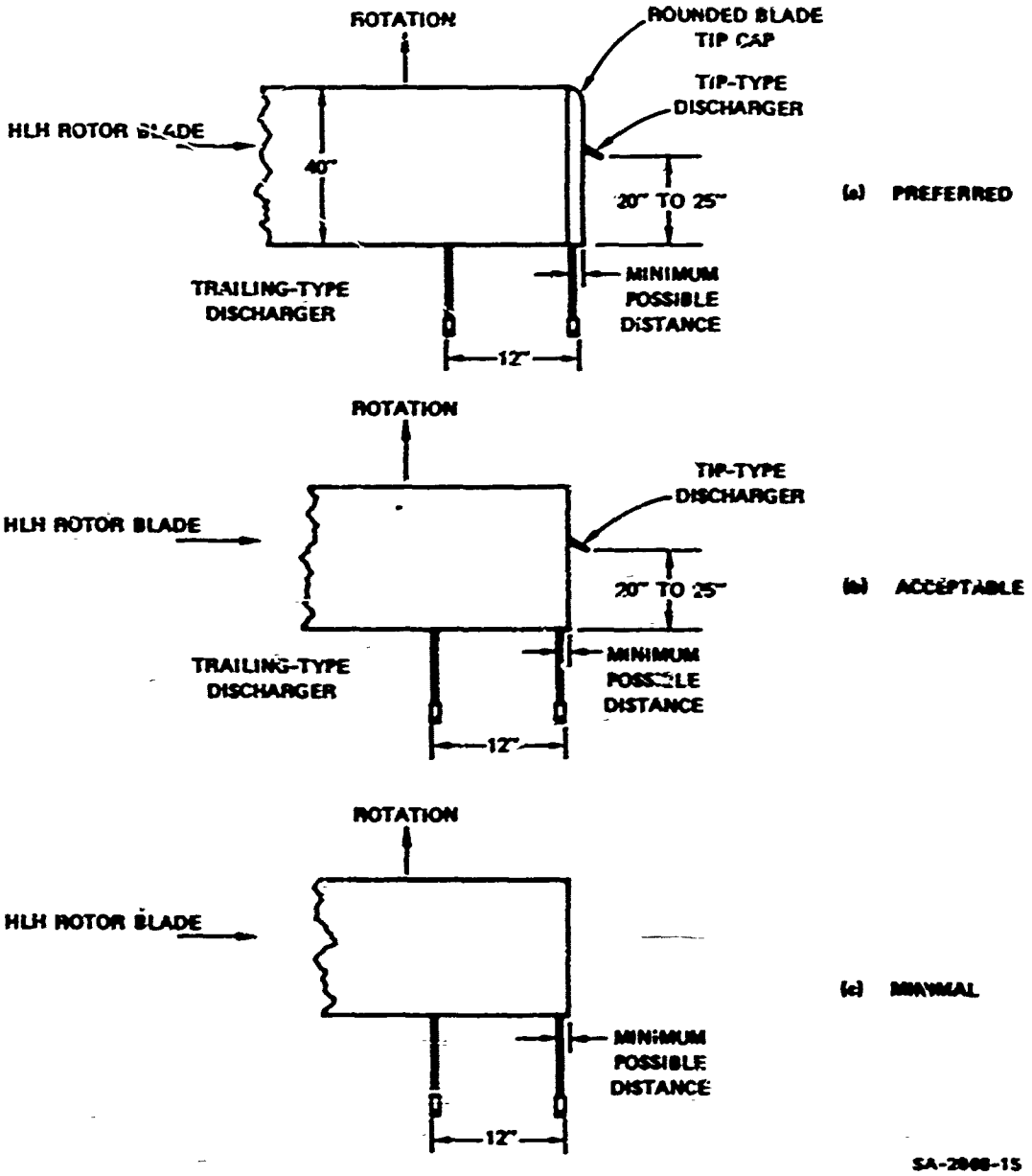

FIGURE 14 RECOMMENDED DISCHARGER INSTALLATIONS ON HLH BLADES

the rounded tip exposes the sharp edges along the top and bottom of the blade tip If it is possible for vortexes with their associated localized pressure reductions to occur at any of these sharp corners, the threshold may be reduced sufficiently that corona will occur at potentials below 100 kV. Before the design of Figure 14(b) can be considered seriously, it should be ascertained that vortices are not likely to occur in any of the regions of high electric field at the blade tip. If, for example, a two-to-one pressure reduction is conceivable as the result of vortex generation, the design of Figure 14(b) will be highly marginal.

The minimum possible discharger installation is shown in Figure 14(c). Here two trailing dischargers are installed on each blade with no provision for tip-type dischargers to inhibit corona from the sharp corners on the tip itself. This design has the merit of requiring no rework of the blade tips, and incorporates only trailing-type dischargers. The results of the model studies conducted on the present program coupled with experience gained on conventional jet aircraft flight tests indicates that the design of Figure 14(c) is not likely to be satisfactory. The sharp corners on the blade tips will be highly prone to corona at voltages comparable to those required to discharge the expected currents from the HLH. Attempting to increase the current-handling capability of the design of Figure 14(c) by adding more trailing dischargers will be only marginally productive because additional dischargers after the first one or two add smaller increments of discharging capability (see Figure 42 of Ref. 8). It should be observed at this time that the reason for using tip-type dischargers is not that they add greatly to the current discharged. Rather, they are used to generate a column of space charge behind them to increase the corona threshold of the region in which they are installed, thereby preventing unwanted, noise-producing corona from occurring on the aircraft structure in these regions.

IV BLADE-COATING TESTS

Evaluation of the adequacy of the candidate rotor-blade coating systems was carried out using the SRI tribcelectric charging facility shown in Figure 15. In this facility, a flow of particulate material (lycopodium powder) is directed onto the surface of the sample under

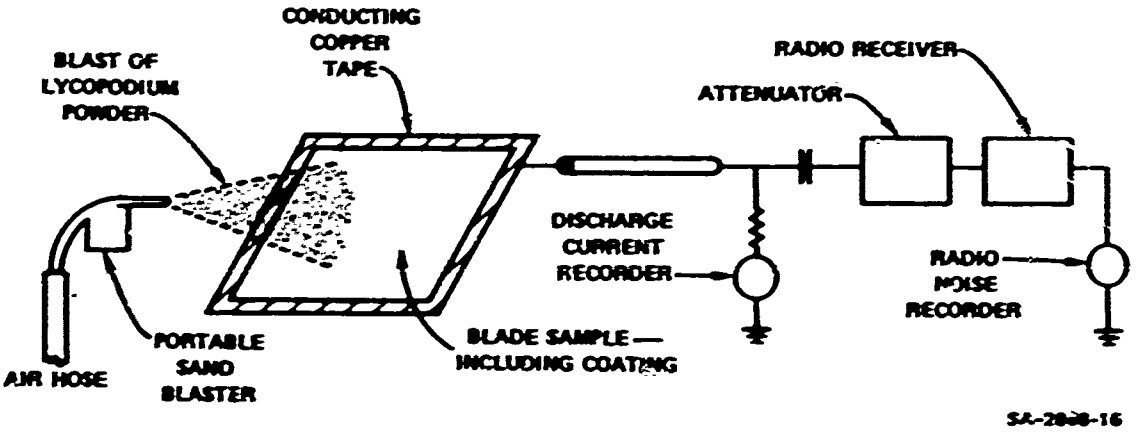

FIGURE 15 TEST SETUP USED IN BLADE-COATING TESTS

test. Frictional charging resulting from the impact of the particles on the test surface charges the surface in the same way as dust or ice crystals would charge the rotor-blade surface. Charging current density is measured by monitoring the current arriving on the conducting ring surrounding the target. In the tests, the currents ranged from 2 to 6 $\mu A/ft^2$. At 6 $\mu A/ft^2$, only 100 ft^2 of blade area would be required to generate the maximum current of 600 μA postulated for the HLH. Thus it is felt that the tests were adequately severe. By darkening the room, it was possible to observe the occurrence of streamer discharges on the surface of the test sample. The occurrence of streamer discharges

was also detected by the existence of radio noise pulses. These were detected using a radio receiver connected to the metal rim around the periphery of the test sample. The attenuator shown in the receiver system permitted a rough estimate to be made of the degree of noise reduction achieved through the application of a particular conductive coating system.

The strength of the triboelectric charging test is that it simulates all aspects of the plastic charging and discharging processes at the same time. In addition, there are no wires leading to power supplies and no electrodes attached to the test sample to cast doubt on the validity of the tests.

During the test program, 26 samples (some were duplicates) of promising coating systems and bare plastic samples were tested in the triboelectric charging facility. The samples were prepared by Boeing Vertol using materials and techniques acceptable for ultimate use in production.

The details of preparation of the test samples are shown in Figure 16. The samples were prepared by making each successive layer of the coating system smaller than the preceding layer to provide definite access to each of the elements of the test panel. In particular, the test-panel design allowed for the use of a simple scheme for installing a current-collecting electrode around the panel. This was accomplished by placing a strip of copper tape around the rim so that the tape protruded 1/2-inch onto the anti-abrasion layer. In this way the copper tape collected current flowing to ground via the conducting layer as well as current discharged via streamers over the top surface. The upper grounded metal rim in Figure 16 was an aluminum frame installed over the outside of the entire structure to provide a definite form to the electromagnetic coupling fields. This is important to assure reasonable repeatability of the streamer noise pulse measurements. The

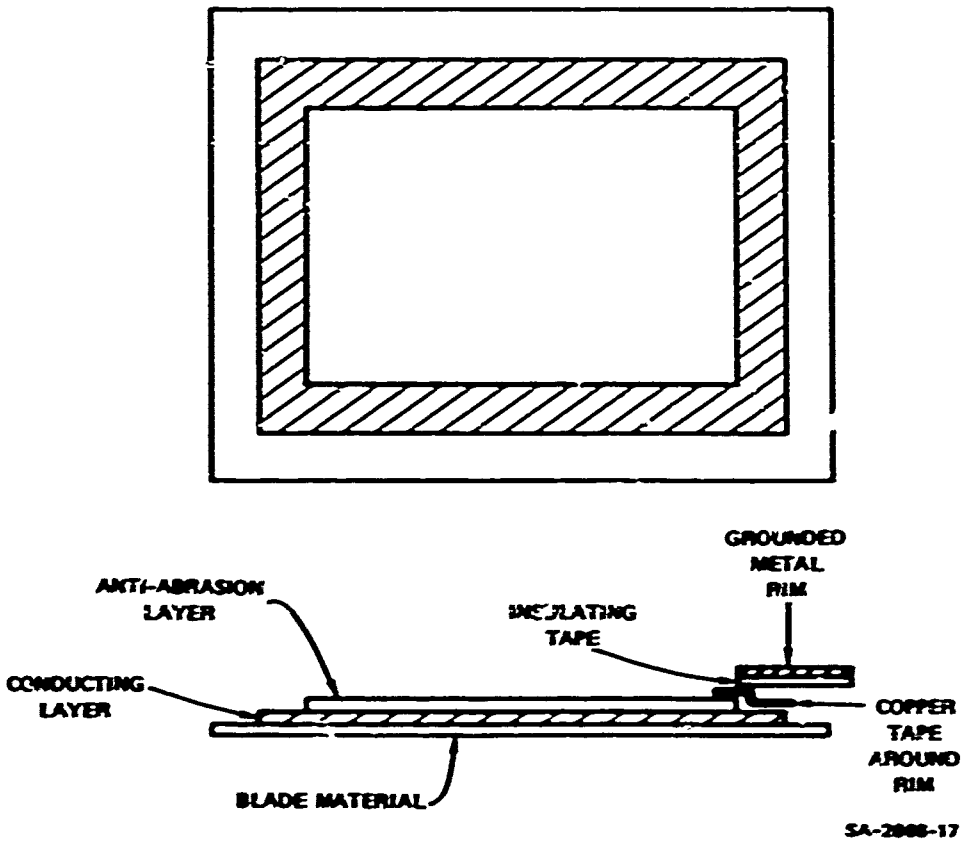

FIGURE 16 TEST-SAMPLE DETAILS

The aluminum frame was sufficiently far back from the inner edge of the copper tape that the rim did not collect any of the dc charging current.

The dust-blowing facility was set up in a room equipped with a dehumidifier and heater. The samples were stored in this room for two days prior to the start of the tests to permit them to dry out thoroughly to eliminate leakage through surface-moisture films. Testing in this environment simulates operation under the low-humidity conditions existing in the desert and in the arctic. During the actual electrification tests, the humidity remained in the range 21% to 28% and the temperature was in the range 84°F to 88°F.

None of the nonconductive coating systems were satisfactory. Under frictional charging, they all produced visible streamer discharges and

high levels of radio noise. The requirements for a satisfactory coating system are discussed in the Appendix. Upon completion of a dust-blowing test, the lycopodium powder used as the charging material was often attracted to the surface of the nonconductive panel, and formed patterns showing the paths taken by streamer discharges originating on the grounded conducting rim around the test panel and propagating out to the center of the panel as shown in Figure 17.

No such dust patterns were observed on any of the satisfactory conductively coated panels. It should also be noted that there was never any noise produced by electrification of any of the best conductively coated panels. The noise-monitoring and recording instrumentation was turned on at the start of each test so that noise occurring at the first electrification could certainly have been detected.

A description of the blade-coating samples tested is given in Table 1. (The film resistivity listed in Table 1 was determined by applying two strips of copper tape on opposite edges of the conducting layer of Figure 16 and measuring the resistance between the two strips using an ohmmeter.) The overall results of the tests are summarized in Table 2. The data are presented in Table 2 so as to permit comparison of the effectiveness of various base materials and their effectiveness in combination with overcoatings of different abrasion-resistant materials. The noisiest samples tested were Numbers 19, 20, 25, and 26 (neither of which incorporated conductive material in its formulation). Accordingly, the noise levels generated by these samples were taken as the 0-dB reference typical of noise generated on an untreated blade, and the noise level observed on all the other samples is expressed as dB below this reference level. Several of the multilayer conductive coating systems were found to be very satisfactory in completely eliminating discharges on the surfaces of the blades. Particularly good were:

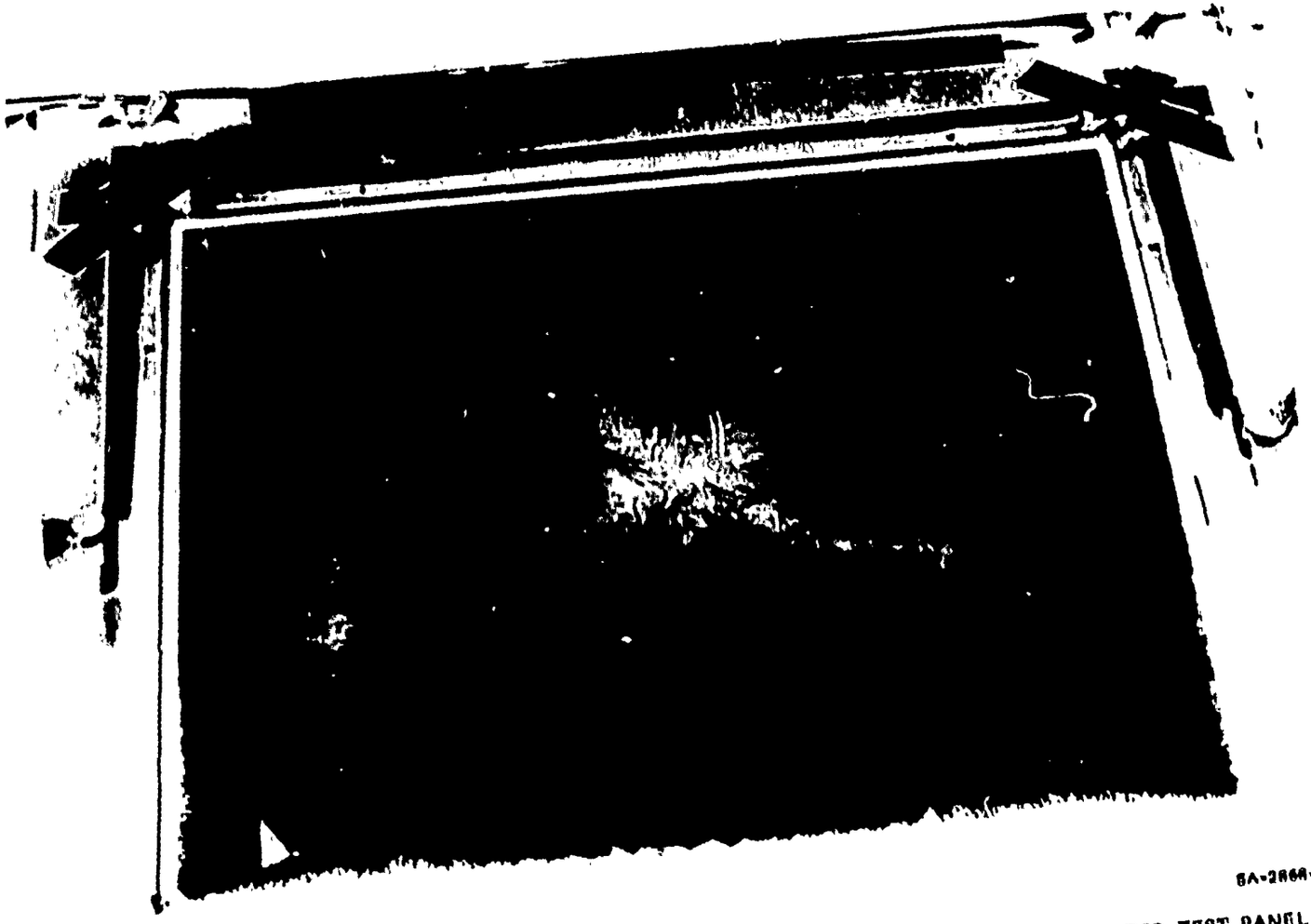

SA-2868-18

FIGURE 17 TRACKS OF STREAMER DISCHARGES GENERATED ON NONCONDUCTIVELY COATED TEST PANEL

Table I

DESCRIPTION OF BLADE-MATERIAL TEST-PANEL COATINGS

Sample Number	Coatings	Coating Thickness (inch)	Measured Conductance Film Resistivity (Ω/□)
1, 2	BMS 10-21 conductive coating-epoxy, black	0.0014-0.0017	2.8×10^{6}
	MIL-C-83286 Polyurethane coating (34082 green) plus BA-2 additive	0.0017-0.0023	3.2×10^{6}
3, 4	BMS 10-21 conductive coating-epoxy, black	0.0004-0.0018	6×10^{4}
	MIL-C-83286 Polyurethane coating (34082 green)	0.0017-0.0023	7.2×10^{6}
5, 6	BMS 10-21 conductive coating-epoxy, black	0.0004-0.0018	10.8×10^{6}
	MIL-C-22750 epoxy coating (34087 olive drab) plus BA-2 additive	0.0024-0.0028	3.9×10^{6}
7, 8	BMS 10-21 conductive coating-epoxy, black	0.0004-0.0015	4.2×10^{6}
	MIL-L-19538 acrylic nitrocellulose lacquer (34087 olive drab) plus BA-2 additive	0.002-0.0025	4.8×10^{6}
9, 10	(Planned for HLH blade)		
	BMS 10-21 conductive coating-epoxy, black	0.0004-0.0018	6×10^{6}
	MIL-P-23377 epoxy primer	Mist coat	—
	MIL-L-19538 acrylic nitrocellulose lacquer (34087 olive drab)	0.002-0.0025	3.6×10^{6}
11, 12	(Considered for UTDAS blade)		
	BMS 10-21 conductive coating-epoxy, black	0.0004-0.0018	6.3×10^{6}
	MIL-C-22750 epoxy coating (34087 olive drab)	0.0024-0.0028	7.2×10^{6}
13	Magna S-B-6 conductive coating-polyurethane, black	0.002-0.004	7×10^{6}
	MIL-P-23377 epoxy primer	Mist coat	—
	MIL-C-83286 polyurethane coating (34087 olive drab)	0.0017-0.0023	—
14	Magna S-B-6 conductive polyurethane coating, black	0.002-0.004	20×10^{6}
	MIL-P-23377 epoxy primer	Mist coat	—
	MIL-C-83286 polyurethane coating (34082 green)	0.0017-0.0023	—
15, 16	Magna S-B-6 conductive coating, black	0.002-0.004	28×10^{6}
	MIL-P-23377 epoxy primer	Mist coat	17×10^{6}
	MIL-C-22750 epoxy coating (34087 olive drab)	0.0024-0.0028	—
17, 18	Magna S-B-6 conductive coating, black	0.002-0.004	7×10^{6}
	MIL-P-23377 epoxy primer	Mist coat	6×10^{6}
	MIL-L-19538 acrylic nitrocellulose lacquer (34087 olive drab)	0.002-0.0026	—
19, 20	(Used for CH-46 overhaul)		
	MIL-P-23377 epoxy primer	0.0006-0.0009	—
	MIL-L-19538 acrylic nitrocellulose lacquer (34087 olive drab)	0.002-0.0026	—
21, 22	(Used on UTDAS)		
	MIL-P-23377 epoxy primer	0.0006-0.0009	—
	MIL-C-22750 epoxy coating (34087 olive drab)	0.0024-0.0028	—
23, 24	(A.F. Polyurethane)		
	MIL-P-23377 epoxy primer	0.0006-0.0009	—
	MIL-C-83286 polyurethane coating (34082 green)	0.0017-0.0023	—
25, 26	(Used on CH-47)		
	MIL-C-8514 wash primer	0.0002-0.0004	—
	MIL-L-7178 lacquer primer	0.0003-0.0005	—
	MIL-L-19538 acrylic nitrocellulose lacquer (34087 olive drab)	0.002-0.0026	—

Table 8

RESULTS OF BLADE-SAMPLE CHANGING STUDIES

Blade Base-Coat Material / Blade Top-Coat Material		Polyurethane Mil-C-83286	Polyurethane + EA 2 Mil-C-83286 Plus RA 2	Epoxy Mil-C-22750	Epoxy + EA 2 Mil-C-22750 Plus RA 2	Epoxy Primer Mil-P-23377 Acrylic Nitrocellulose Lacquer Mil-L-19538	Acrylic Nitrocellulose Lacquer + EA 2 Mil-L-19538 Plus RA 2	Epoxy Primer + Acrylic Nitrocellulose Lacquer Mil-P-23377 Plus Mil-L-19538	Epoxy Primer + Polyurethane Mil-P-23377 Plus Mil-C-83286	Epoxy Primer + Epoxy Coating Mil-P-23377 Plus Mil-C-22750	Lacquer Primer + Acrylic Nitrocellulose Lacquer Mil-L-7962 Plus Mil-L-19538
BMS 10-21 (conductive)	Sample Number	3, 4	1, 2	11, 12	5, 6	9, 10	7, 8				
	Noise Reduction (dB)	34, >40	>40	29, 19	24, 20	>40	37, >40				
Magna 8-H-0 (conductive)	Sample Number							17, 18	13, 14	15, 16	
	Noise Reduction (dB)							>40	>40	>40, 19	
Mil-C-8514 (Wash primer)	Sample Number										25, 26
	Noise Reduction (dB)										0
None	Sample Number							19, 20	23, 24	21, 22	
	Noise Reduction (dB)							0	19	0	

- BMS 10-21 + polyurethane + RA-2 (Samples 1 and 2).
- BMS 10-21 + Epoxy Primer + Acrylic Nitrocellulose Lacquer (Samples 9 and 10).
- Magna 8-B-6 + Epoxy Primer + Acrylic Nitrocellulose Lacquer (Samples 17 and 18).
- Magna 8-B-6 + Epoxy Primer + Polyurethane (Samples 13 and 14).

It is interesting to note that Samples 7 and 8 are not as reliably quiet as Samples 9 and 10, although the main difference between the two sets of samples is that 7 and 8 have RA-2 added to the lacquer top coat. On the other hand, Samples 1 and 2, incorporating RA-2, are quieter than Samples 3 and 4, which have the same formulation without RA-2.

In applying the results shown in Table 1, it should always be borne in mind that outstanding coating systems produced no <u>detectable</u> noise in the measuring system used, and showed no indication of charge accumulation or streamering. It is possible, therefore, that the noise reductions achieved were substantially in excess of 40 dB. The effort to shield and otherwise improve the measuring system to increase its dynamic range was beyond the scope of the present contract. Until more carefully controlled measurements can be made, however, it is safer not to try splitting hairs concerning the data of Table 2 by arguing that one system is only a few dB better than another. Instead, it should be concluded that four of the systems (listed above) produced no detectable streamer noise under frictional charging, while the rest produced noise of greater or lesser degree.

The results of the streamer-noise calculations, shown in Figures 4 through 7, indicated that streamer noise on the blades must be reduced by over 40 dB to bring it down to the daytime-atmosphere level. Thus there is no merit in considering paint systems that cannot provide this degree of noise reduction.

In an effort to determine why some of the coating systems were more satisfactory than others, it was argued that one possible mechanism leading to the observed noise-reduction differences could be molecular interactions between the conductive substrate and the insulating, abrasion-resistant top coat that affected the insulating and voltage-breakdown characteristics. It was felt that evidence of these interactions and their effects could be gained by measuring the electrical conductivity of the various surfaces. Accordingly, an experiment to measure the conductivity of the blade-panel coating-system samples was designed.

The experiment used a coaxial resistance measuring probe illustrated in Figure 18. A coaxial design was chosen because, with this structure, all current flow is confined between the inner and outer conductors. Thus, accurate measurement of resistance is possible even near the edges of panels. The dimensions of the coaxial probe were chosen so that the conductivity (in ohms/□) of any surface could be determined by multiplying the measured resistance by 4. In order to obtain uniform surface contact over the entire probe, soft, conducting vinyl pads were applied to the brass contact pads of the probe. These pads had side-to-side resistances of less than 1 ohm.

Initial measurements revealed that several of the panel samples showed a surprisingly high conductivity at low (1.5 volt) voltages. Further testing, performed under the same temperature and humidity conditions as described earlier, shows that all of the panel samples with the BMS 10-21 base material gave high conductivity at low voltages.

Since the abrasion-resistant top coatings on these panels are generally nonconducting, the materials were suspect and a microscopic examination of the panels was made. Figure 19 shows a photograph of the surface of panel Sample No. 7 magnified 10 times. It can be seen from the photograph that the surface is irregular. A microprobe attached to

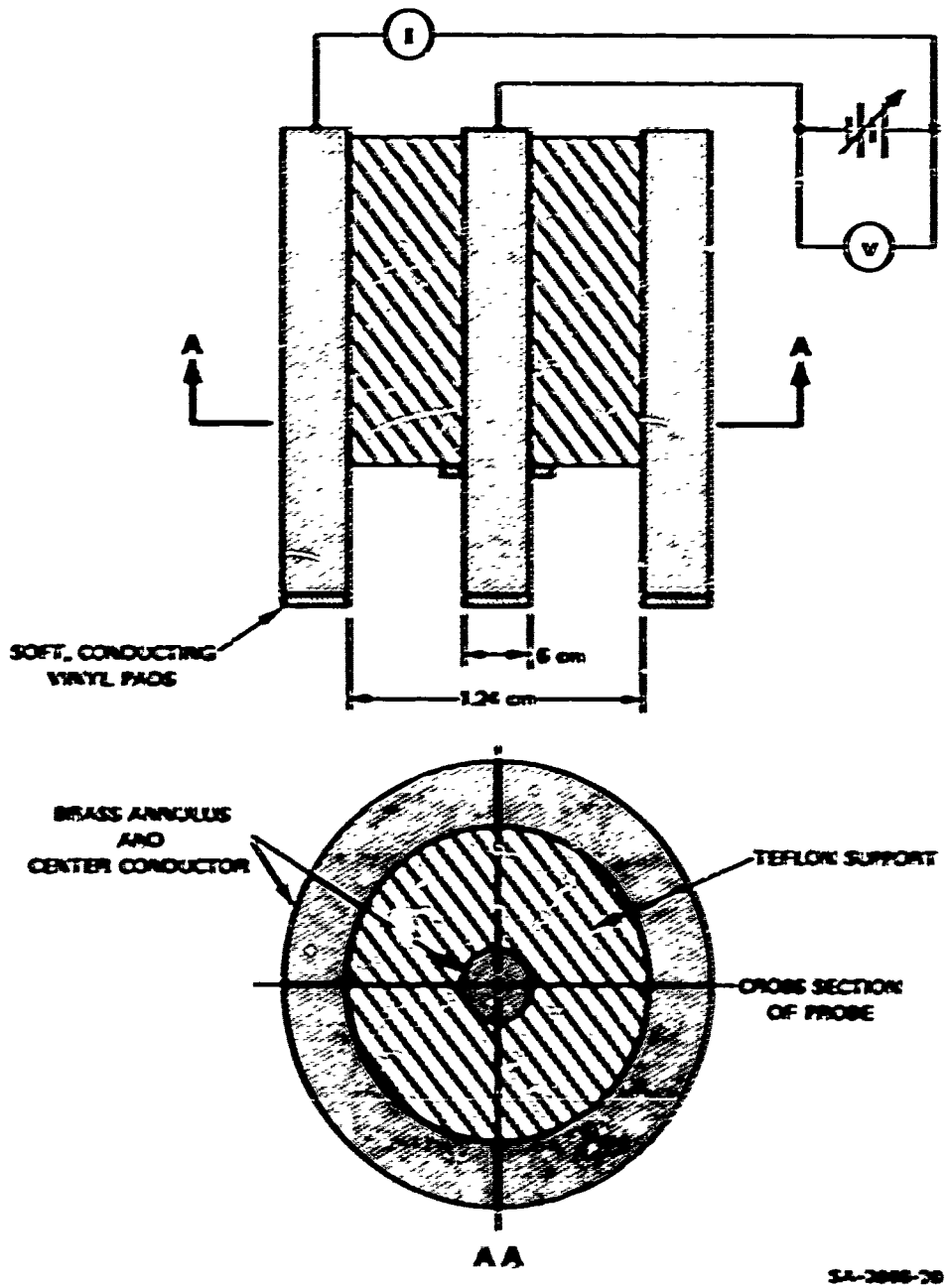

FIGURE 18 COAXIAL CONDUCTIVITY PROBE USED TO DETERMINE THE ELECTRICAL CONDUCTIVITY OF VARIOUS HLH BLADE PANELS

FIGURE 19 PHOTOGRAPH OF TYPICAL BLADE SAMPLE WITH BMS 10-21 BASE MATERIAL (100)

an ohmmeter revealed that the "smooth" valleys shown in the photograph were nonconductive while the "mountainous" lumps on the surface were conductive, even when touched with the slightest pressure. These "lumps" are evidently the BMS 10-21 base coat, which had erupted through the top coat, leading to the high values of conductivity (low resistance) measured by the coaxial probe. Figure 20 shows a photograph of one of the "mountains" observed on Sample 2 at 30X magnification. This "mountain," while being somewhat larger than most, was not atypical of those observed.

Table 3 shows the results of the surface-resistivity measurements made on the panels with the BMS 10-21 base coat. Each resistivity value shown in the figure is the average of five measurements on each panel. It can be seen that there is a high degree of correlation between the

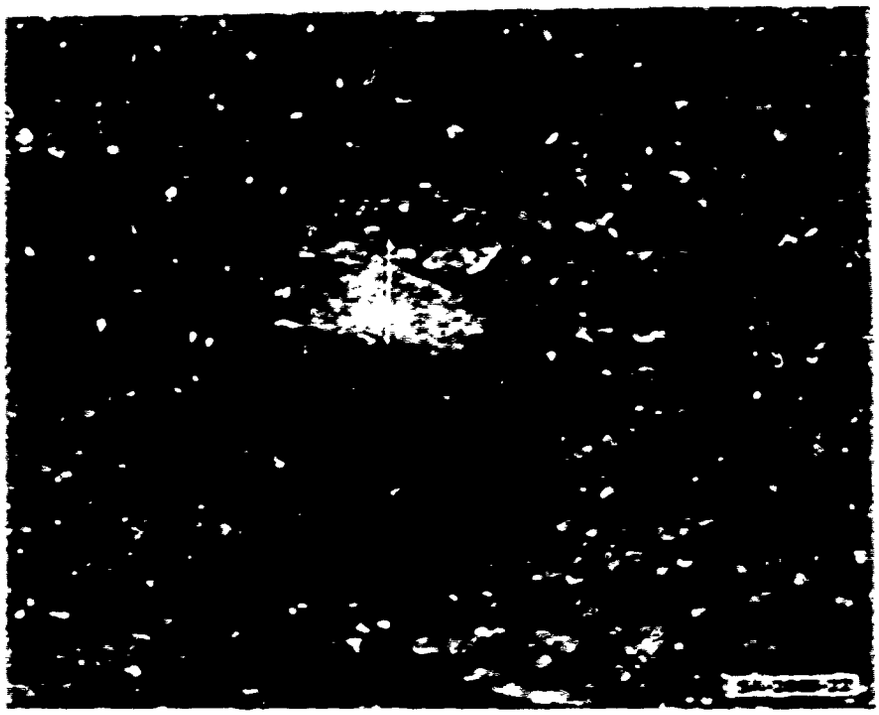

FIGURE 20 PHOTOGRAPH OF SURFACE OF SAMPLE 2 [illegible]

measured surface conductivity and the noise reduction afforded by each coating system.

Table 3

COMPARISON OF NOISE REDUCTION AND SURFACE RESISTIVITY OF PANELS WITH RMS 10-21 BASE COAT

Sample Number	Noise Reduction (dB)	Surface Resistivity (Ω/□)
1, 2	>40	900
3, 4	34, >40	400
5, 6	24, 20	1200
7, 8	37, >40	300
9, 10	>40	200
11, 12	29, 19	= to 1200

The measured resistivity data also are consistent with a general description of the surface. To the observer it appears that the panels with a high conductivity (and good noise reduction) were the roughest (and consequently had the greatest exposure of conductive base material). Another qualitative observation made while the panels were being examined was that the top-coat materials over the BMS 10-21 base coat were easily scratched, and seemed softer than the other top-coat materials tested.

The remaining panels--those with the Magna 8-B-6 base material, and the panels with no conductive base coat--were similarly examined under a microscope and subjected to a low- and high-voltage conductivity measurements. These panels exhibited no measurable conductivity at low voltages, so high-voltage measurements were made. The results of these measurements are shown in Figure 21 together with noise-reduction data from Table 2. It can be seen from this figure that the data form three distinct conductivity groups. It is also evident from the figure that there is a high degree of correlation between conductivity and noise reduction.

Figure 22 shows a photograph of the surface of Sample 18, magnified 10 times. This panel has an epoxy top coat and the Magna 8-B-6 base. This surface was typical of all panels with the Magna base coat. It can be seen that the surface is very smooth, with no irregularities. The surface was moderately hard, resisting easy scratching.

It was calculated from these tests that the Magna 8-B-6 base coat covered with either the Mil-P-23377 plus Mil-L-19538, or the Mil-P-23377 plus Mil-C-83286 abrasion-resistant coatings were superior to the other coating systems from the standpoint of noise reduction and mechanical properties of the surface.

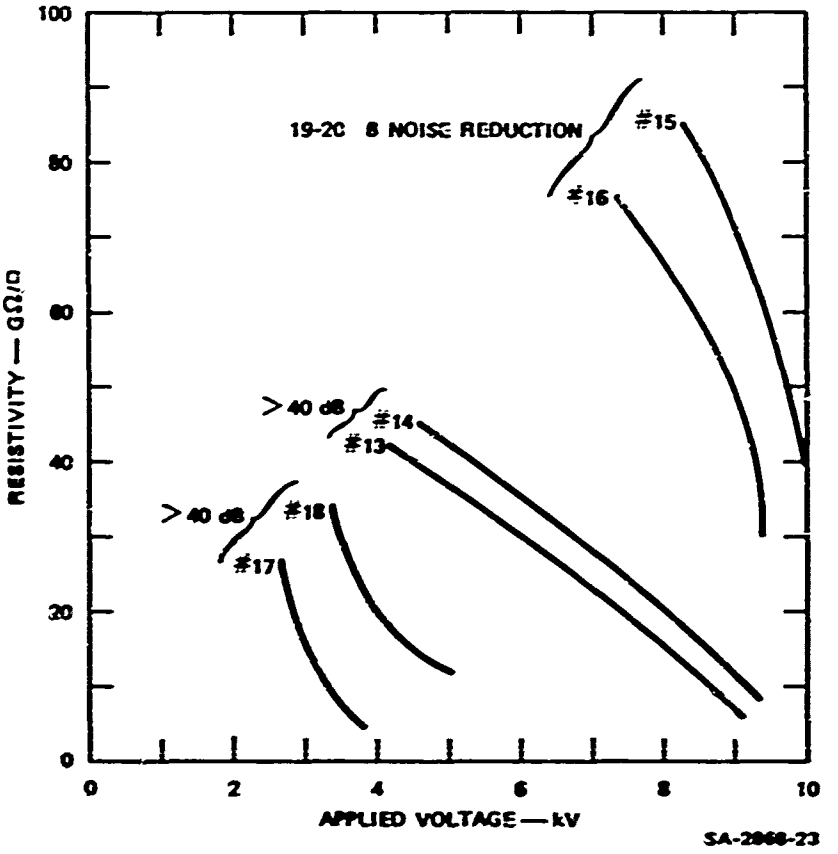

FIGURE 21 HIGH-VOLTAGE CONDUCTIVITY OF HLH BLADE PANELS WITH MAGNA 8-8-6 BASE MATERIAL

It was further concluded from these tests that the low- or high-voltage conductivity measurements could be a viable technique for checking noise suppression on the HLH blades in a field environment.

Some of the other considerations important in designing a streamer-free surface are discussed in the Appendix.

FIGURE 22 PHOTOGRAPH OF TYPICAL HLH BLADE PANEL SURFACE WITH MAGNA 8-8-6 CONDUCTIVE BASE COAT

V CONCLUSIONS AND RECOMMENDATIONS

An analysis was made to determine the noise to be expected at typical LF and HF antenna locations on an unmodified HLH helicopter. This analysis, based on previous work substantiated by flight testing on conventional aircraft, indicates that noise stemming from corona discharges from the blade tips or from streamer discharges across the plastic blade surfaces will produce interference levels 40 dB or more above daytime atmospheric noise. The LORAN-D System designer can achieve improved system performance until he has reduced his system input noise figure to the atmospheric noise level. From this observation it can be inferred that such systems are now, or ultimately will be, operating at the atmospheric-noise-level limit. This means that the predicted corona or streamer noise from the blades will severely degrade the performance of such a system. In particular, the analysis indicates that 40 dB of noise reduction is required to reduce the electrostatically generated noise levels to the daytime atmospheric level.

Electrostatic-model studies of the HLH helicopter indicate that it is possible to devise a passive-discharger installation for the helicopter blades that will handle the maximum anticipated discharge current of 600 μA predicted for the HLH helicopter while providing 45 to 60 dB of corona-noise reduction. Various discharger arrangements on the blades were considered in light of probable aerodynamic conditions at the blade tips. The one recommended for use on the HLH is based on presently best available information regarding maximum expected pressure reductions in the vortices generated at the corners of the blade tips.

The results of charging tests conducted on candidate conductive-coating systems for the blades indicated that four of the coating systems

tested were highly successful in eliminating corona discharges on the blade surface. The dynamic range of the setup used was such that noise reductions greater than 40 dB could not be specified quantitatively. When the four successful coating systems were tested, however, no noise whatsoever was observed in the test setup. It is recommended that one of the four successful coating candidates be selected and applied to the blades of the HLH helicopter. The application of this treatment will provide the required 40-dB streamer-noise reduction needed to approach the atmospheric noise limit.

In connection with the conductive-coating-system tests, it was found that two systems that were essentially identical, except for the addition of an additive in one of the layers, produced markedly different noise reduction. It was speculated that the differences might stem from differences in the ease with which the top layer of the coating system punctures electrically. In order to pursue this question, and to identify the "better" of the good panels, a measurement was made of the surface conductivity of each candidate panel using a special, coaxial, surface-conductivity probe.

These measurements revealed a definite correlation between the conductivity and noise suppression afforded by the different coating systems. The panels with high conductivity showed good noise suppression, while the panels with low conductivity demonstrated poorer noise-suppressing capabilities.

A microscopic examination of the panel surfaces showed that the panels with the BMS 10-21 base coat had irregular surfaces with what appeared to be eruptions of the base-coat material through the top-coat layer. Since the panels sub-coated with Magna 8-B-6 did not have these eruptions, but some of them exhibited good noise reduction, it is suggested that the Magna 8-B-6 base coat is superior to the BMS 10-21

because the Magna 8-B-6 appears to result in a tougher coat. No measurements of abrasion resistance were actually made during the present program, however.

These measurements also showed that a conductivity measurement could easily be adapted for an "on-site" quality-control technique to determine the noise-suppressing capabilities of an HLH blade while it was mounted on the helicopter.

Appendix

REQUIREMENTS FOR ELECTRICALLY CONDUCTIVE BLADE COATINGS

1. General

The surfaces of helicopter blades are made of insulating plastic materials. In operation, these surfaces acquire electrostatic charge, which ultimately results in electrical breakdowns to metallic structures of the blade. These breakdowns generate radio noise that can disable communication and navigation systems on the helicopter. The breakdowns can be avoided by drawing away the charge as rapidly as it arrives. This can be accomplished by making the plastic sufficiently conductive or by applying a conductive film over the plastic blade surface. Often it is necessary to use a double-layer coating system because the conducting material is too fragile to withstand the abrasion of normal helicopter operation.

2. Single-Layer Conductive Coating

It is of interest to calculate the maximum value of the surface resistance that can be used before the electric field at the surface of the plastic becomes high enough to result in air breakdown. Let us consider a surface on which charging is occurring as shown in Figure A-1. Charging current density $J_c = 50 \times 10^{-6}$ A/ft^2 $\cong 500 \times 10^{-6}$ A/m^2 is arriving on the surface in question. This causes current to flow along the surface to the grounded conducting rim. At a distance r from the center, we will have a total current crossing the boundary of

$$I(r) = J_c \pi r^2 \qquad \text{(A-1)}$$

Pages 50, 51 and 52 are Blank.

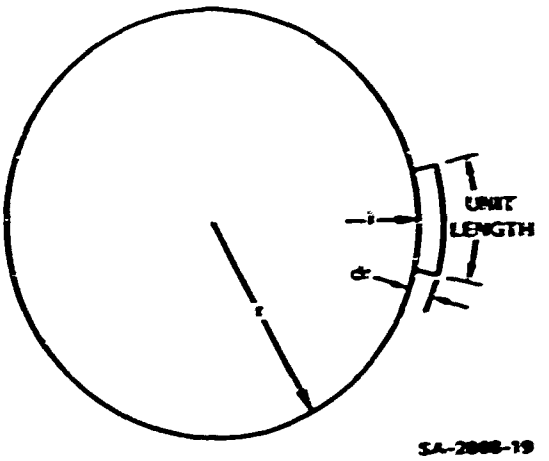

FIGURE A-1 CURRENT FLOW IN SURFACE CONDUCTING FILM

The current per unit distance i around the circumference of this boundary is

$$\frac{I(r)}{\ell} = \frac{J_c \pi r^2}{2\pi r}$$

$$= j_c \, r/2 \quad . \qquad \text{(A-2)}$$

The voltage drop this current generates in the infinitesimal distance dr is

$$dV = \frac{I(r)}{\ell} R \, dr \qquad \text{(A-3)}$$

where R is the surface resistivity in ohms per square. By definition, the electric-field intensity caused by this current flow is, from Eq. (A-3),

$$E(r) = \frac{dV}{dr} = \frac{I(r)}{\ell} R \quad . \qquad \text{(A-4)}$$

Substituting Eq. (A-2) into Eq. (A-4) we obtain

$$E(r) = J_c \, r \, R/2 \quad . \tag{A-5}$$

Solving Eq. (A-5) for R

$$R = \frac{2E(r)}{J_c r} \quad . \tag{A-6}$$

If we specify the maximum field intensity we can tolerate before air breakdown occurs over the surface of the blade and define the charging-current density, Eq. (A-6) defines the maximum permissible value of surface resistivity.

Air breakdown occurs at sea-level pressure when $E = 3 \times 10^6$. Let us assume that $r = 0.5$ m (a rather large surface). Recalling that we said $J_c = 500 \times 10^{-6}$ A/m^2, and substituting these values into Eq. (A-6), we obtain

$$R = \frac{3 \times 10^6 (2)}{500 \times 10^{-6} (0.5)}$$

$$= 2.4 \times 10^{10} \ \Omega/\square \quad .$$

To allow for some safety margin, let us say that we require R = 1000 megohms per square.

It is of interest to see what this surface resistivity implies regarding the bulk resistivity of the material compromising the conducting surface film. The surface resistivity is related to the bulk resistivity by

$$R = \frac{\rho}{t} \tag{A-7}$$

where t is the film thickness. Assuming a film thickness of t = 0.001 inch = 2.5×10^{-3} cm, and R = 10^{10} ohms per square, we find from Eq. (A-7) that the bulk resistivity required in the surface material is

$$\rho = 10^{10}(2.5 \times 10^{-3})$$

$$= 2.5 \times 10^{7} \text{ ohm cm} \quad .$$

3. Double-Layer Conductive Coating

In considering the possible options for helicopter-blade treatment it is evident that one has the choice of making an abrasion-resistant conductive coating, or of applying a more fragile coating and covering it with a thin layer of transparent abrasion-resistant material that either conducts or breaks down, at low voltage levels, to the conducting layer underneath. Let us now consider the two-layer system in which a relatively fragile conducting film is applied over the blade surface and this is then covered with a more abrasion-resistant layer. The outer layer must be carefully chosen. If it is not, the system will not function properly.

Ideally, if the outer anti-abrasion coating material is a good insulator, it should be sufficiently imperfect that reasonably closely spaced holes exist between the outside of the coating and the conducting layer underneath. A thin film that is likely to have voids appears to be a good first choice. Less energy is required to puncture a thin film, and a thin film when punctured probably would suffer less damage and generate less radio noise than would a thick layer of material.

Instead of assuming that the outer anti-abrasion layer is a perfect insulator, it is of interest also to consider the case of an anti-abrasion layer with some bulk electrical conductivity. Surface charge will still

accumulate on the outside surface, and a high electric field will exist inside the outer layer, but now we will have some current flow through the top layer to the conducting film. Let us consider a region of anti-abrasion material having a surface area A and a thickness ℓ. The current I arriving on this area is

$$I = JA \tag{A-8}$$

where J is the surface-charging-current density. The resistance R from the top surface to the conducting film is given by

$$R = \frac{\rho \ell}{A} \tag{A-9}$$

where ρ is the bulk resistivity of the anti-abrasion-layer material. The voltage drop V across the conducting anti-abrasion layer is given by Ohm's law,

$$V = IR \quad , \tag{A-10}$$

We want to make certain that this voltage appearing across the anti-abrasion layer does not exceed the dielectric strength E_{max} of the material defined by

$$E_{max} = \frac{V_{max}}{\ell} \quad . \tag{A-11}$$

Substituting Eqs. (A-8) and (A-9) into Eq. (A-10), and then substituting Eq. (A-10) into Eq. (A-11) we find

$$E = JA \frac{\rho \ell}{A} \frac{1}{\ell} \quad . \tag{A-12}$$

Solving Eq. (A-12) for the bulk resistivity we obtain

$$\rho_{max} = \frac{E_{max}}{J} \qquad (A-13)$$

which tells us the bulk resistivity needed to permit the anticipated charging-current density J to flow through the anti-abrasion coating without exceeding the dielectric strength of the coating. (The foregoing arguments presume that the anti-abrasion layer is very thin so that all of the fields produced by the static charging are normal to the plane of the conducting film underneath).

It will be interesting to use Eq. (A-13) to calculate a typical value of bulk resistivity required to meet our criterion of allowing the current to flow through the anti-abrasion sheet without puncturing it. In the flight tests described in Refs. 6 through 9, it was found that surface charging currents can reach values as high as 50 $\mu A/ft^2$, so that $J = 5.4 \times 10^{-8}$ A/cm^2. Let us assume that the anti-abrasion layer is made of some material having a dielectric strength similar to that of a piece of glass 1 mm thick for which $E_{max} = 2.5 \times 10^5$ to 5.5×10^5 V/cm[11]. Substituting these numbers into Eq. (A-13) we find $\rho_{max} = 4.6 \times 10^{12}$ to 10^{13} ohm cm. These resistivities are several orders of magnitude lower than those published for many of the modern plastic materials used in formulating paints, accordingly it will be necessary to either choose the paint material carefully or to load the paint with conductive material.

REFERENCES

1. E. G. Enche, "Precipitation Static Interference," Proc. IRE, Vol. 27, No. 5 (May 1939).

2. R. C. Ayers and J. O. Jarrard, "Aircraft Precipitation Static Investigation," Contract W 33-106 SC-70, Trans-World Airlines, Inc. (August 1944).

3. R. Gunn et al., "Army-Navy Precipitation Static Project," Proc. IRE, Vol. 34, Nos. 4 and 5 (1946).

4. E. J. Dana, "Block and Squirter for Reduction of Precipitation Static," Report 15, Second Air Force Operations Analysis (February 1945).

5. R. L. Tanner, "Radio Interference from Corona Discharges," Tech. Report 37, Contract AF 19(604)-266, SRI Project 591, Stanford Research Institute, Menlo Park, Calif. (April 1953).

6. R. L. Tanner and J. E. Nanevicz, "Radio Noise Generated on Aircraft Surfaces," Final Report, Contract AF 33(616)-2761, SRI Project 1267, Stanford Research Institute, Menlo Park, Calif. (September 1956).

7. J. E. Nanevicz, "A Study of Precipitation-Static Noise Generation in Aircraft Canopy Antennas," Tech. Report 62, Contract AF 19(604)-1296, SRI Project 1197, Stanford Research Institute, Menlo Park, Calif. (December 1957).

8. R. L. Tanner and J. E. Nanevicz, "Precipitation Charging and Corona-Generated Interference in Aircraft," APCRL 336, Tech. Report 73, Contract AF 19(604)-3458, SRI Project 2491, Stanford Research Institute, Menlo Park, Calif. (April 1961), AD-261 029.

9. J. E. Nanevicz, E. F. Vance, R. L. Tanner, and G. R. Wilbers, "Development and Testing of Techniques for Precipitation Static Interference Reduction," ASD-TR-62-38, Final Report, Contract AF 33(616)-6561, SRI Project 2848, Stanford Research Institute, Menlo Park, Calif. (January 1962), AD-272 807.

10. R. L. Tanner and J. E. Kaneviez, "An Analysis of Corona-Generated Interference in Aircraft," Proc. IEEE, Vol. 52, No. 1, pp. 44-52 (January 1964).

11. J. E. Kaneviez and R. L. Tanner, "Some Techniques for the Elimination of Corona Discharge Noise in Aircraft Antennas," Proc. IEEE, Vol. 52, No. 1, pp. 53-64 (January 1964).

12. "Passive Null Field Discharges for CH-54 Aircraft," ESSURE Item No. 265, U.S. Army Vietnam, Long Binh, Republic of Vietnam (U).

13. M. C. Becher, "CH-54A Static Discharge Test Program Evaluation of Dynasciences Active ESD and Granger Passive P-Stat Dischargers," DCR-299, Dynasciences Corporation (Scientific Systems Division). Blue Bell, Penn. (16 April 1969).

14. M. C. Becher, "Investigation of CH-54A Electrostatic Charging and of Active Electrostatic Discharger Capabilities," U.S. Army Aviation Material Laboratories, Fort Eustis, Virginia (January 1970).

15. M. E. Insleman et al., "Ensure 265 CH-54 (Flying Crane) Electrostatic Discharger Evaluation," Technical Report ECOM-3120, U.S. Army Electronics Command, Ft. Monmouth, N. J. (April 1969).

16. J. E. Kaneviez and D. G. Douglas, "Electric Discharge System," Final Report, Contract CE-700377, SRI Project 1657, Stanford Research Institute, Menlo Park, Calif. (November 1972).

17. D. G. Douglas and J. E. Kaneviez, "Flight Test Evaluation of Helicopter Cargo-Handling Systems—Passive Static-Electricity Drainage," Contract DAAJ01-71-C-0890, Order No. CE-702049 SRI Project 2590, Stanford Research Institute, Menlo Park, Calif. (September 1973).

18. J. T. Bolljohn, "Antennas For Airborne ADF Systems" Final Report, Task II, Contract AC-33(615)-83, Stanford Research Institute, Menlo Park, Calif. (July 1964).

19. Reference Data For Engineers, 4th Ed., p. 762 (International Telephone and Telegraph Corporation, New York, N.Y., 1956).